AD-A158 867 HYPERVELOCITY PLASMAS WITH STRONG MHD (MAGNETOHYDRODYNAMIC) INTERACTIONS(U) STD RESEARCH CORP ARCADIA CA S T DEMETRIADES ET AL DEC 84 STDR-84-29 1/1

UNCLASSIFIED AFOSR-TR-85-0667 F49620-83-C-0115 F/G 20/9 NL

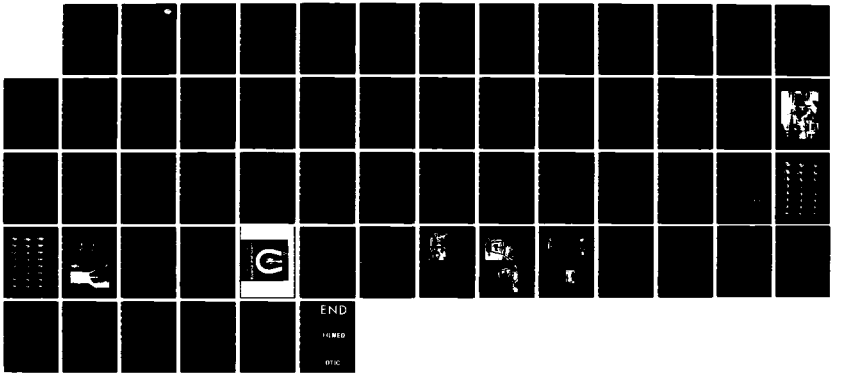

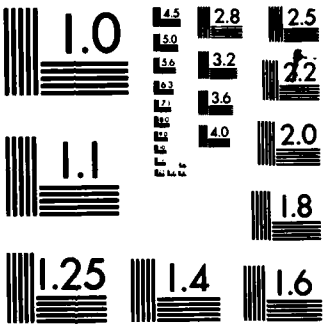

MICROCOPY RESOLUTION TEST CHART
NATIONAL BUREAU OF STANDARDS-1963-A

AFOSR-TR- 85 0667

STD RESEARCH CORPORATION

POST OFFICE BOX "C", ARCADIA, CALIFORNIA 91006
TELEPHONE: (213) 357-2311

STDR-84-29

FINAL TECHNICAL REPORT

HYPERVELOCITY PLASMAS WITH STRONG MHD INTERACTIONS

S. T. DEMETRIADES
PRINCIPAL INVESTIGATOR

Period Covered: 1 June 1983 - 31 May 1984

December 1984

STD Research Corporation
P.O. Box "C"
Arcadia, California 91006

Prepared Under
USAF, AFSC
Air Force Office of Scientific Research
Building 410
Bolling AFB, Washington, DC 20332-6448
Major Henry L. Pugh
Under Contract F49620-83-C-0115

UNCLASSIFIED

SECURITY CLASSIFICATION OF THIS PAGE (When Data Entered)

REPORT DOCUMENTATION PAGE	READ INSTRUCTIONS BEFORE COMPLETING FORM
1 REPORT NUMBER: STDR-84-29	2. GOVT ACCESSION NO.: AD-A158867
	3. RECIPIENT'S CATALOG NUMBER:
4 TITLE (and Subtitle): HYPERVELOCITY PLASMAS WITH STRONG MHD INTERACTION	5. TYPE OF REPORT & PERIOD COVERED: Final Technical Report 1 Jun '83 - 31 May '84
	6. PERFORMING ORG. REPORT NUMBER: STDR-84-29
7. AUTHOR(s): S.T. Demetriades and C.D. Maxwell	8. CONTRACT OR GRANT NUMBER(s): F49620-83-C-0115
9. PERFORMING ORGANIZATION NAME AND ADDRESS: STD Research Corporation, P.O. Box C, Arcadia, CA 91006	10. PROGRAM ELEMENT, PROJECT, TASK AREA & WORK UNIT NUMBERS: Project No. 2301/A7
11. CONTROLLING OFFICE NAME AND ADDRESS: Air Force Office of Scientific Research, Bolling AFB, Washington DC, 20332-6448	12. REPORT DATE: December 1984
	13. NUMBER OF PAGES: 54
14. MONITORING AGENCY NAME & ADDRESS(if different from Controlling Office)	15. SECURITY CLASS. (of this report): Unclassified
	15a. DECLASSIFICATION/DOWNGRADING SCHEDULE

16. DISTRIBUTION STATEMENT (of this Report)

Approved for public release; distribution unlimited

17. DISTRIBUTION STATEMENT (of the abstract entered in Block 20, if different from Report)

18. SUPPLEMENTARY NOTES

(unclassified)

19. KEY WORDS (Continue on reverse side if necessary and identify by block number)

Magnetohydrodynamics, hypervelocity plasmas; high-interaction, high Reynolds number; simulation codes; validation experiments.

20. ABSTRACT (Continue on reverse side if necessary and identify by block number)

Use of body forces to inject energy into a plasma offers certain advantages over simple energy addition by Ohmic heating. To achieve ever-increasing levels of energy per unit mass by this strategy requires detailed and thorough understanding of high-interaction magnetohydrodynamics (HIMHD) through realistic computer simulation. Such simulation is possible by the existing, unique STD Research Corporation HIMHD codes provided they undergo further

DD FORM 1 JAN 73 1473 EDITION OF 1 NOV 65 IS OBSOLETE S/N 0102 LF 014 6601

UNCLASSIFIED

SECURITY CLASSIFICATION OF THIS PAGE (When Data Entered)

A

20. Abstract

validation in the high-interaction regime through systematic experiments. The present work has carried out a critical assessment of several methods for achieving high-interaction high-magnetic Reynolds number MHD flows. It indicates that continuous flow (as contrasted to pulsed flow) plasmajet-driven MHD devices offer the greatest advantages and potential for validating the STD/MHD codes at high MHD interaction over a wide range of parameters with the greatest confidence. It has led to the definition of specific plasmajet-driven experiments, utilizing existing equipment, as the most effective way to carry out this task.

STDR-84-29

FINAL TECHNICAL REPORT

HYPERVELOCITY PLASMAS WITH STRONG MHD INTERACTIONS

S. T. DEMETRIADES
PRINCIPAL INVESTIGATOR

Period Covered: 1 June 1983 - 31 May 1984

December 1984

STD Research Corporation
P.O. Box "C"
Arcadia, California 91006

Prepared Under
USAF, AFSC
Air Force Office of Scientific Research
Building 410
Bolling AFB, Washington, DC 20332-6448
Major Henry L. Pugh
Under Contract F49620-83-C-0115

ABSTRACT

Use of body forces to inject energy into a plasma offers certain advantages over simple energy addition by Ohmic heating. To achieve ever-increasing levels of energy per unit mass by this strategy requires detailed and thorough understanding of high-interaction magnetohydrodynamics (HIMHD) through realistic computer simulation. Such simulation is possible by the existing, unique STD Research Corporation HIMHD codes provided they undergo further validation in the high-interaction regime through systematic experiments. The present work has carried out a critical assessment of several methods for achieving high-interaction, high-magnetic Reynolds number MHD flows. It indicates that continuous flow (as contrasted to pulsed flow) plasmajet-driven MHD devices offer the greatest advantages and potential for validating the STD/MHD codes at high MHD interaction over a wide range of parameters with the greatest confidence. It has led to the definition of specific plasmajet-driven experiments, utilizing existing equipment, as the most effective way to carry out this task.

HYPERVELOCITY PLASMAS WITH STRONG MHD INTERACTIONS

TABLE OF CONTENTS

LIST OF FIGURES

FINAL TECHNICAL REPORT STDR-84-29

HYPERVELOCITY PLASMAS WITH STRONG MHD INTERACTIONS

1. INTRODUCTION

Emerging Air Force mission needs require major advances in space power and propulsion technology AFOSR recognition of these needs has resulted in a new "Space Power and Propulsion Initiative". Leading candidate devices to meet these needs, such as magnetoplasmadynamic (MPD) thrusters and magnetohydrodynamic (MHD) generators, involve the interaction of partially ionized conducting gases (plasma) with strong electromagnetic fields. To minimize weight and maximize performance of such MPD/MHD devices requires strong coupling of the fluid to the electromagnetic forces, in other words, strong electromagnetic interaction.

Analysis and computer simulation of high-velocity partially ionized plasma under conditions of strong electromagnetic-fluid interactions has received little attention to date. The internationally recognized numerical simulation capabilities of STD Research Corporation have been developed to include the capability of calculating the behavior of a fluid which is strongly coupled to electromagnetic forces. However, only limited opportunity to explore strongly coupled cases has been possible under the STD Research Corporation contracts that provide numerical simulations support to the MHD program of DOE/NASA and the Navy Pulsed Power MHD generator project. This has resulted from a combination of both funding limitations and the pressing need to provide an understanding of the ongoing MHD experiments which to date have been limited to modest strength

magnetohydrodynamic interactions. Thus, no venturesome and bold applications of the numerical simulation tools of STD Research have been made.

Even in the devices studied to-date, with modest levels of magnetohydrodynamic interaction, results of numerical simulations have uncovered significant new phenomena, which can have major impact on performance and can lead to the invention of revolutionary techniques and devices. Such phenomena include generation of secondary flows, which in turn cause major nonuniformities in the electrode current and heat transfer and boundary layer separation leading to stall of the MHD generator, stagnation pressure asymmetries, short-duration high-voltage spikes and other electromagnetic pulse-like effects. Investigation of design improvements to minimize such effects and maximize performance can be accomplished with numerical simulations at a small fraction of the cost of tests in appropriate generator test facilities.

The continuing growth in computer capability and the concurrent continuing reduction in computation costs will inevitably broaden the use of numerical simulation in engineering design and development. Already these developments have had a major impact on aircraft design approaches. In advanced space power and propulsion systems, where hardware and facilities to test at very high power will be very expensive, numerical simulations to minimize required testing and to permit larger systems and reliable scaling of small facility test data will be even more important.

The credibility of models used in numerical simulations can only be validated by comparison with critical definitive

experiments. The program initiated by the present work is intended to provide such a definitive validation of the extension of the STD numerical simulation capability into the range of strong MHD interactions and moderate-to-high magnetic Reynolds numbers.

Various types of experiments could be utilized for this validation, including a steady-state MHD generator operating into a space-simulated vacuum exhaust or a high power MPD arc. In the proposal to AFOSR dated April 1982 (STDR-UP-003-82) that led to the work reported here, STD Research Corporation proposed a specific pulsed, explosive-driven, MHD (XMHD) generator experiment which offered a, possibly, minimal cost approach to obtain the desired conditions of strong or very strong magnetohydrodynamic interactions. However, subsequent analysis of the capabilities of this device showed that it did not live up to expectations for two reasons:

(a) Although it does represent a minimal-cost approach for achieving significant MHD interactions, because of the short times involved, the instrumentation costs for data acquisition beyond the simplest current-voltage history (e.g. measurements of flow non-uniformity) are prohibitive.

(b) The range of test conditions such as magnetic Reynolds numbers and interaction parameters that can be achieved at reasonable cost is not as wide as can be achieved with other MHD devices for the same cost.

In the course of the present work, a comparison of various devices for achieving high MHD interaction at relatively high magnetic Reynolds number, including the explosive-driven MHD (XMHD) generator, proved that the continuous plasma-jet driven

MHD devices offer the widest range of interaction parameters at the highest magnetic Reynolds numbers (i.e. the highest product Rm x S_u x I_p where S_u is the interaction parameter based on velocity and I_p is the interaction parameter based on pressure).

The resulting validated simulation capability will stimulate and accelerate inventiveness in the field of plasma devices for Air Force requirements. It can help develop flightweight accelerators producing focused jets with velocities of the order of 10^6 m/sec and particle densities of the order of 10^{25} per m^3; and flightweight power generators producing either 1 to 10 megawatts for hours (10^{10} to 10^{11} joules in 10^4 secs) or 100 to 1000 gigawatts for 10-100 microseconds (10^6 to 10^8 joules in 10^{-5} to 10^{-4} sec) with high repetition rates.

2. OBJECTIVES AND STATUS

The main objective of the present work was to define appropriate experiments for the validation of the STD Research MHD computer codes at high MHD Interactions (of the order of interaction parameters of 10 or higher), where the emerging Air Force interests lie (e.g., aerospace mass accelerators or space power generator applications).

To accomplish this objective, progress was also required in understanding the flow distortions associated with strong MHD interactions in hypervelocity plasmas.

The present work has accomplished the above objectives. A detailed formulation of a sound approach to achieve the validation objectives stated above has been achieved, and it has been presented in a technical paper at the AIAA 22nd Aerospace Sciences Meeting. This paper, which is part of the present report as Appendix A, describes the technical results of the main tasks of this work.

The results and status of the present work can be summarized by reviewing the Figures 3 and 4 of Appendix A.

Figure 3 of Appendix A is a plot of the magnetic Reynolds number, Rm, as a function of the interaction parameter based on velocity, S_u, for twelve linear MHD devices. At least nine of these devices have been built and tested experimentally (albeit not all at their highest interaction levels).

Figure 4 of Appendix A is a plot of the magnetic Reynolds number, Rm, as a function of the interaction parameter based on pressure, I_p, for the same devices.

The pattern that emerges from a study of Figures 3 and 4 of Appendix A is clear: The products Rm x S_u x I_p, Rm x S_u and Rm x I_p, as well as the parameters S_u and I_p, all reach their maximum values with the Demetriades-type (References 1 - 6) devices which consist of an arc-jet generated plasma passing through an MHD section (i.e. a section where MHD body forces can be applied either to accelerate or decelerate the plasma) and exhausting into a vacuum chamber. Operation of these devices ranges from many seconds (if there is no special cooling and large currents, averaging 1,000 amperes/cm^2 or higher, are applied) to continuous (if magnetic fields are applied to generate moderate current densities, of the order of 100 amperes/cm^2). The conductivity of the plasma in these devices ranges from hundreds of mhos per meter to tens of thousands of mhos per meter depending on the arc-jet enthalpy and the use or non-use of preionizing electrodes, seed, etc. They can be used as generators or accelerators and the principal investigator has experience with building dozens of these devices to operate in the 5 - 100 Kw, 50 - 200 Kw and 100 - 1,000 Kw power levels. These devices are described in detail in References 1 - 13.

Progress in understanding the theory of these devices through the STD/MHD codes has made it possible to seek quantitative answers and uses for a multitude of formerly little-understood effects such as the magnetoaerothermal effect, electrode shorting, arcing and erosion at high interaction parameters, plasmajet deflection, etc.

Specifically, the use of these devices as the main source of experimental data makes it possible to vary or measure (over a very wide range and pretty much independently), the following quantities (and, where applicable, their distributions):

(1) Composition of working fluid,
(2) Enthalpy of plasma and gas temperature,
(3) Electron temperature,
(4) Magnetic field,
(5) Current density and total current,
(6) Flow velocity,
(7) Mass flow rate,
(8) Ratio of Hall to Faraday current,
(9) Heat flux to the walls,
(10) Applied or induced voltage,
(11) Flow static and stagnation pressure,
(12) Degree of excitation of various species,
(13) Plasma conductivity,
(14) Electrode composition, configuration, erosion and temperature
(15) Reaction forces on magnet and other parts of the device due to acceleration or deceleration (thrust and/or drag) as well as many other parameters.

All the components for this plasma flow facility exist in storage at STD Research Corporation. It will be necessary, however, to reassemble them. A schematic of the reassembled facility is shown in Figures 1 and 2. A photograph of the assembled equipment is shown in Figure 3.

Use of this continuous plasma flow High Interaction MHD (HIMHD) facility will provide answers to the main objective of validating the STD/MHD codes by direct observation and measurement of effects predicted by these codes. Some of these effects are boundary layer stall and jet deflection due to the magnetoaerothermal effect, plasma focusing and compression effects, etc. These effects and their method of determination or measurement are described in References 6, 7, 12, 14 and 15.

In addition, specific solutions will be provided to the following problems that still plague the engineers and experimenters in this area at strong MHD interaction:

(1) Electron emission and absorption from materials in dense plasmas with and without magnetic fields (surface effects).

(2) Core and boundary-layer turbulence and related effects such as boundary-layer stall and flow separation in MHD (interface and bulk effects).

(3) High interaction effects in the core of the MHD flow-field such as secondary flows (bulk effects).

(4) Electrode erosion, arcing, shorting, aging enhancement and current leakage (surface plus interface effects).

(5) Power take off, electrode consolidation and equipotential exploitation by boundary layer compensation in MHD devices (aiming to get rid of electrode consolidation circuits).

(6) Optimum conductivity and analytic expressions for the power of continuous MHD devices at any Rm (as opposed to pulsed MHD devices).

3. RECOMMENDATIONS FOR THE VALIDATION EXPERIMENTS

At least two unambiguous and uncompromising experiments can be carried out quite easily with the available HIMHD equipment to test the STD HIMHD computer codes. One experiment consists of applying a magnetic field across the stabilized arc-generated jet of plasma (either with simultaneously applied electric currents or, by shorting the electrodes of Figure 1, with an induced current) and observing the angle of deflection of the jet. This deflection angle is due to the Hall current and related secondary flows and is known to exist (References 12, 15 - 19 and Appendix A) in HIMHD devices. The other experiment consists of an MHD generator designed to operate between the static pressure furnished at the exit of the plasma jet (between 2 and 0.1 atmospheres) to the vacuum tank pressure (between 0.001 and 0.0001 atmospheres) and observing the point at which boundary layer over the anode stalls (e.g. due to the magnetoaerothermal effect) and the flow begins to separate. This stall is known to be caused by HIMHD effects and has been observed (References 15 and 17 - 19).

An additional argument for the second experiment on generator stall is the following: It is alright to talk, on paper, about space applications of MHD generators with enthalpy extraction of 25% or more. It is well known that the higher the pressure ratio over which an MHD generator works, the higher the enthalpy extraction. However, the STD/HIMHD codes show that the more the MHD flow is slowed down and the faster it is slowed down, the more likely it is that it will separate through boundary layer stall. What is (a) the rate (e.g. with distance down the channel) at which energy can be removed from the flow in an MHD generator and (b) the amount of energy that can be removed before the generator stalls? What is the optimum trade-off

between energy density and expansion ratio? Clearly, an infinitely long MHD channel is an absurdity. Where do we cut it off for space applications?

The calculation of these two effects in detail and the comparison of the detailed computations with the experiments should furnish the necessary and sufficient proof required to use the STD/MHD codes with confidence in high MHD interaction regimes.

The approach formulated above for the validation of the STD/MHD codes at high interaction presents the following advantages compared to the original approach we had contemplated in the proposal, STD-UP-003-83 of April 1983, for the present work:

(1) The facility operating envelope is wider with respect to achievable interaction parameters, magnetic Reynolds numbers, and pressure ratios.

(2) More parameters can be measured and more data points with the same time resolution can be acquired in a continuous facility in the experiment time available.

(3) Safety precautions are less demanding.

(4) Visual observations are more readily available.

(5) Flow chemistry may be made as simple or as complex as necessary for valid simulations.

(6) More efficient use of available manpower.

The experiments that we are proposing here have been used at STD Research Corporation for many years. In fact, the basic techniques have been described in Reference 1. For ease of reference, we are attaching Reference 1 as Appendix B to this report.

The parameters that can be measured in these experiments with the instrumentation now available at STD Research Corporation are indicated in References 20 - 24, where also the available STD continuous plasma flow facility (STD/CPFF) and its operating envelope are described.

4. CONTRIBUTING PROFESSIONAL PERSONNEL

The following professional personnel were associated with the research effort reported herein:

1. S. T. Demetriades - Principal Investigator
   [A.B., Physics-Mathematics-Chemistry, Bowdoin College, 1950; M.S., Chemical Engineering, Massachusetts Institute of Technology, 1951; M.E. (Professional Degree in Mechanical Engineering) California Institute of Technology, 1958.]
2. C. D. Maxwell - Associate Principal Investigator
   [B.S., Physics, California Institute of Technology, 1968.]
3. R. Blankenhorn - Staff Scientist
   [B.S. and M.S., Theoretical Physics, University of Innsbruck, Austria, 1971; Ph.D. in Physics and Computer Sciences, University of Innsbruck 1982.]
4. C. D. Bangerter - Staff Scientist
   [B.S., Physics, University of Utah, 1960; Graduate Courses, Physics, University of Washington, 1960; Graduate Courses, Physics, University of Utah, 1961, 1962; Plasma Physics, Brigham Young University, 1961, 1962.]
5. D. A. Oliver - Chief Scientist
   [B.S., Mechanical Engineering, University of Santa Clara, 1961; M.S. and Ph.D. degrees, Stanford University, 1963 and 1967, respectively.]
6. J. E. Holman - Research Engineer
   [B.S., Chemical Engineering, California Institute of Technology, 1982.]
7. D. W. Early - Programmer, MHD Technology Group
   [B.S., Astronomy, California Institute of Technology, 1976.]
8. J. T. Demetriades - Programmer/Technician (part-time)
   [B.S., Computer Sciences, Loyola Marymount University, 1984.]
9. G. R. Seikel - Staff Scientist (part-time)
   [B.S., 1955, and M.S., 1957, Aeronautical Engineering, University of Notre Dame.]

5. INTERACTIONS - PRESENTATIONS

As mentioned above, the main results of the present program were presented at the 22nd AIAA Aerospace Sciences Meeting (AIAA Paper 84-0155 "Strong MHD Interaction" by S. T. Demetriades and C. D. Maxwell). This paper created significant interaction with other workers in this field who are increasingly utilizing the STD/MHD code results to understand and interpret the results of their experiments (e.g., Stanford University and AVCO Everett Research Laboratories). In addition, this paper pointed out a common error in extrapolating low Magnetic Reynolds Number results: it showed that the total power to the load, P_L, varies like the $\tanh \frac{Rm}{2}$, which approaches an asymptotic limit for $Rm > 3$. Investigators (e.g., Reference 25) who use the low magnetic Reynolds number approximation to this relationship (i.e. $P_L \sim Rm$) will be disappointed in their performance expectations as they push velocity and electrical conductivity to extreme values.

REFERENCES

[1] S. T. Demetriades, "Experimental Magnetogasdynamic Engine for Argon, Nitrogen and Air," ASRL-TM-60-23, Norair Division, Northrop Corporation, presented at 2nd Symposium on Engineering Aspects of Magnetohydrodynamics, University of Pennsylvania, 9-10 March 1961; (Engineering Aspects of Magnetohydrodynamics) Columbia University Press, 1962, pp. 19-44.

[2] S. T. Demetriades and R. W. Ziemer, "Energy Transfer to Plasmas by Continuous Lorentz Forces," ASG-TM-61-37, Norair Division, Northrop Corporation; also presented at the Fourth Biennial Gas Dynamics Symposium, Northwestern University, Evanston, Illinois, 23-25 August 1961, ARS preprint No. 2002-61 also in Magnetohydrodynamics, edited by A. B. Cambel, T. P. Anderson, M. M. Slawsky, Northwestern University Press, 1962, pp. 185-202.

[3] S. T. Demetriades and R. W. Ziemer, "Direct Thrust and Efficiency Measurements of a Continuous Plasma Accelerator," ARS Journal, Vol. 31, No. 9, pp. 1278-1280, September 1961.

[4] S. T. Demetriades and R. W. Ziemer, "Acceleration of Plasmas by Continuous Linear Lorentz Forces," J. Inst. Aerospace Sc., Vol. 29, No. 5, pp. 603-604, May 1962.

[5] S. T. Demetriades and R. W. Ziemer, "Measurements of Electrode Drag and Conductance in a Supersonic Free Jet of Plasma," The Physics of Fluids, Vol. 4, No. 12, p. 1568, December 1961.

[6] S. T. Demetriades, "Novel Method of Measurement of Plasma Properties by Momentum Change Techniques," The Physics of Fluids, Vol. 4, No. 12, pp. 1569-1570, December 1961.

[7] S. T. Demetriades, "Plasma Propulsion," Parts I and II, Astronautics, Vol. 7, Nos. 3 and 4, p. 21 and p. 40, March and April 1962, respectively.

[8] S. T. Demetriades, "Three-Fluid Non-Equilibrium Plasma Accelerators, Part I," presented at ARS Electric Propulsion Conference, 14-16 March 1962, Berkeley, California, ARS Preprint No. 2375-62; reprinted in Progress in Astronautics and Aeronautics, (Electric Propulsion Development), Vol. 9, AIAA Series, pp. 461-511, Academic Press, New York, 1962.

[9] S. T. Demetriades, "Experiments with a High Specific Impulse Crossed-Field Accelerator" presented at the Third Annual Symposium on Engineering Aspects of MHD, University of Rochester, 28-30 March 1962; Gordon & Breach Science Publishers, Inc., New York, New York, pp. 507-525 (1963).

[10] S. T. Demetriades and P. D. Lenn, "Electrical Discharge Across a Supersonic Jet of Plasma in Transverse Magnetic Field," AIAA Journal, Vol. 1, No. 1, pp. 234-236, January 1963.

[11] S. T. Demetriades, P. D. Lenn, J. R. Bodoia, D. L. Ward and G. L. Hamilton, "Three-Fluid Non-Equilibrium Plasma Accelerators, Part II," presented at AIAA Electric Propulsion Conference, 11-13 March 1963, Colorado Springs, Colorado, AIAA Preprint No. 63047.

[12] S. T. Demetriades, "Momentum Transfer to Plasmas by Lorentz Forces," presented at 5th Biennial Gas Dynamics Symposium, Northwestern University, Evanston, Illinois, 14-16 August 1963; published in Physico-Chemical Diagnostics of Plasmas, (T. P. Anderson, R. W. Springer, R. C. Warder, Jr., Editors), Northwestern University Press, Evanston, Illinois, pp. 297-328, November 1963.

[13] S. T. Demetriades, P. D. Lenn, J. R. Bodoia, D. L. Ward and G. L. Hamilton, "Experimental and Analytical Investigations of Crossed-Field Plasma Accelerators. Part I: Report of Major Analytical and Experimental Results," Technical Documentary Report No. ASD-TDR-63-307, May 1963 (ASD-AFSC-USAF-WPAFB, Ohio; Contract No. AF 33(657)-8858). Also Northrop Corporation Report No. NSL 62-113-10, 28 June 1963; Part II of above. Report of All Analytical and Experimental Results. Same date and numbers. Part III of above. Report of High Power Accelerator Tests. Same date and numbers.

[14] S. T. Demetriades and A. N. Kontaratos, "Interaction of a Jet of Plasma with Electric and Magnetic Fields," Applied Scientific Research, Vol. 11, Section B, pp. 335-360 (1964).

[15] S. T. Demetriades, D. A. Oliver, T. F. Swean and C. D. Maxwell, "On the Magnetoaerothermal Instability," Paper AIAA-81-0248, presented at the AIAA 19th Aerospace Sciences Meeting, St. Louis., Missouri, January 12-15, 1981.

[16] S. T. Demetriades, A. A. Vetter, C. D. Maxwell, T. F. Swean, D. A. Oliver and C. D. Bangerter, "The STD/MHD Codes: Comparison of Analysis with Experiments at AEDC/HPDE, Reynolds Metal Co. and Hercules, Inc.," Paper AIAA-81-0173, AIAA 19th Aerospace Sciences Meeting, St. Louis, Missouri, January 12-15, 1981.

[17] S. T. Demetriades, C. D. Maxwell, T. F. Swean, Jr., A. A. Vetter, R. D. Crouse, D. A. Oliver and C. D. Bangerter, "Three-Dimensional Effects in Large Scale MHD Generators," Paper AIAA-81-1231, AIAA 14th Fluid and Plasma Dynamics Conference, Palo Alto, CA, June 23-25, 1981.

[18] S. T. Demetriades, Open Letter to Members of the U. S. MHD Community, including Air Force Office of Scientific Research, on the subject of the Significance of First Confirmation of the Magnetoaerothermal Effect in the Arnold Engineering Development Center High Performance Demonstration Experiment, 25 February 1983.

[19] S. T. Demetriades, C. D. Maxwell, and D. A. Oliver, "Progress in Analytical Modeling of MHD Power Generators II," Proceedings 21st Symposium on Engineering Aspects of Magnetohydrodynamics, Argonne National Laboratory, June 1983, pp. 3.1.1-3.1.20.

[20] S. T. Demetriades, "Determination of Energy-loss Factors for Slow Electrons in Hot Gases," Phys. Rev., Vol. 158, No. 2, pp. 215-217, 10 June 1967.

[21] S. T. Demetriades, "Novel Method for Determination of Energy-loss Factors for Slow Electrons in Hot Gases," STD Research Corporation Report No. STD-68-2, Contract NAS2-3580, (NASA/Ames), Interim Report covering the period 28 April 1966 - 30 June 1968, Accession No. N69-35413, NASA Contractor's Report No. CR-73361, Code 1, Category 24 (August 1968). Available through U. S. Dept. of Commerce, National Bureau of Standards, Clearinghouse for Federal Scientific and Technical Information.

[22] S. T. Demetriades and C. D. Maxwell, "Determination f Energy-loss Factors for Slow Electrons in Hot Gases," STD Research Corporation Report STD-69-1, Final Report Contract NAS2-3580 (NASA/Ames), Accession No. 70-15044, NASA Contractor's Report No. CR 73400 (15 August 1969). Available through U. S. Dept. of Commerce, National Bureau of Standards, Clearinghouse for Federal Scientific and Technical Information.

[23] S. T. Demetriades, G. Fonda-Bonardi and G. S. Argyropoulos, "Experimental Determination of Collision Cross- Sections for Momentum Transfer," U. S. Air Force Office of Scientific Research Final Scientific Report AFOSR 69-2809 TR, USAFOSR, Washington, D. C. 20333 (September 1969).

[24] STD Research Corporation "History, Objectives, Experience, Capabilities," STD Research Corporation, copyright 1980.

[25] S.P. Gill, D.W. Baum, and H. Calvin, "Explosive MHD Research", ARTEC Assoc. Annual Report to ONR, April 1975 - April 1976.

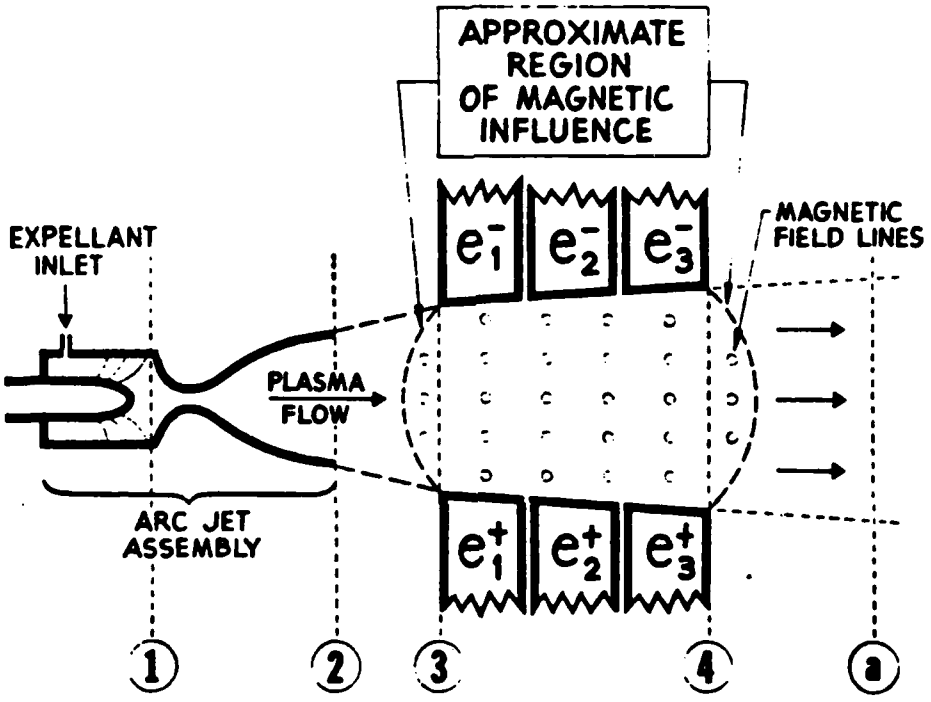

Fig. 1 Schematic of HIMHD Device (generator/accelerator)

4-6918

STD RESEARCH CORPORATION

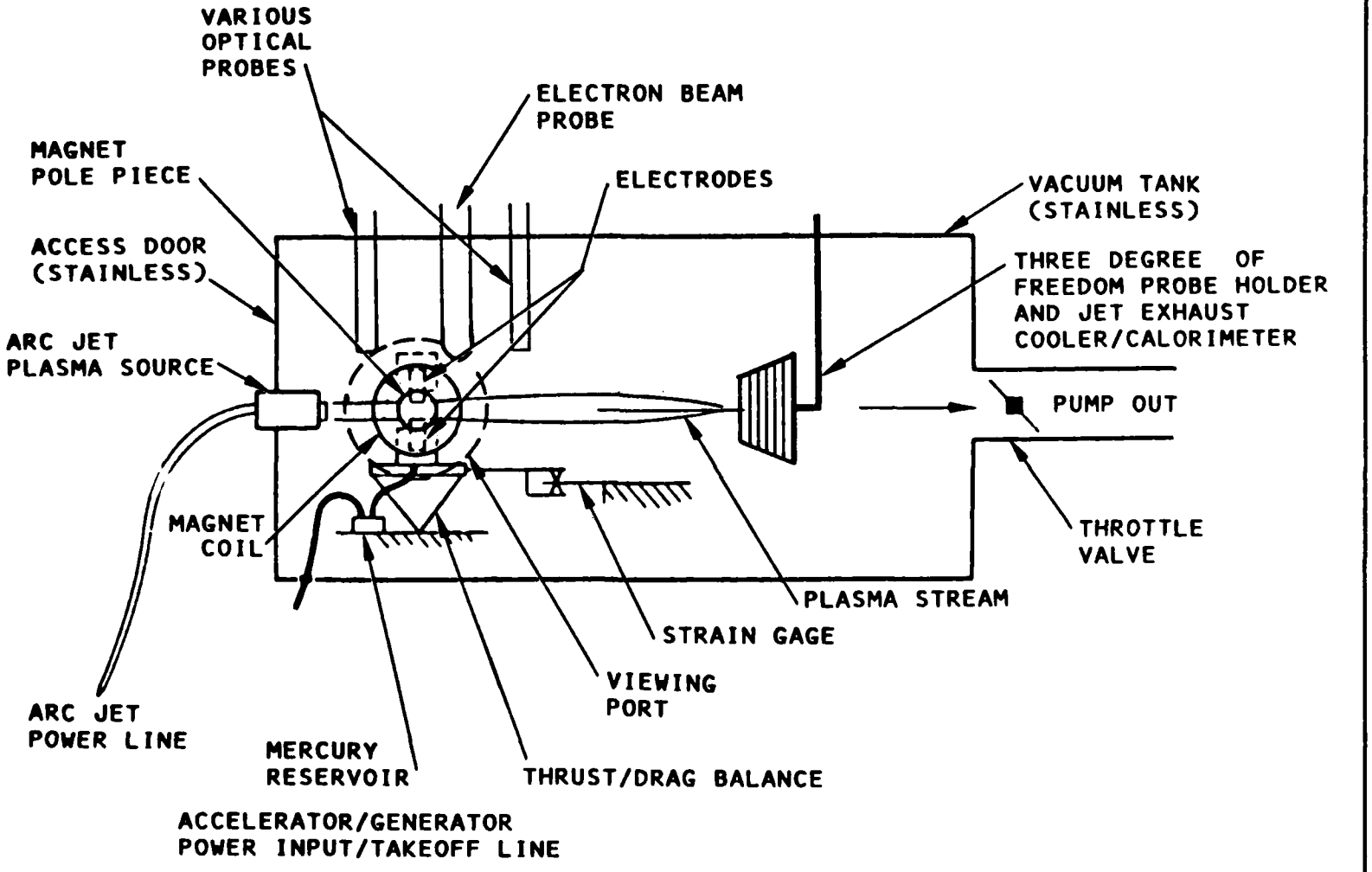

Fig. 2 Schematic of continuous plasma flow HIMHD facility.

4-6916

STD RESEARCH CORPORATION

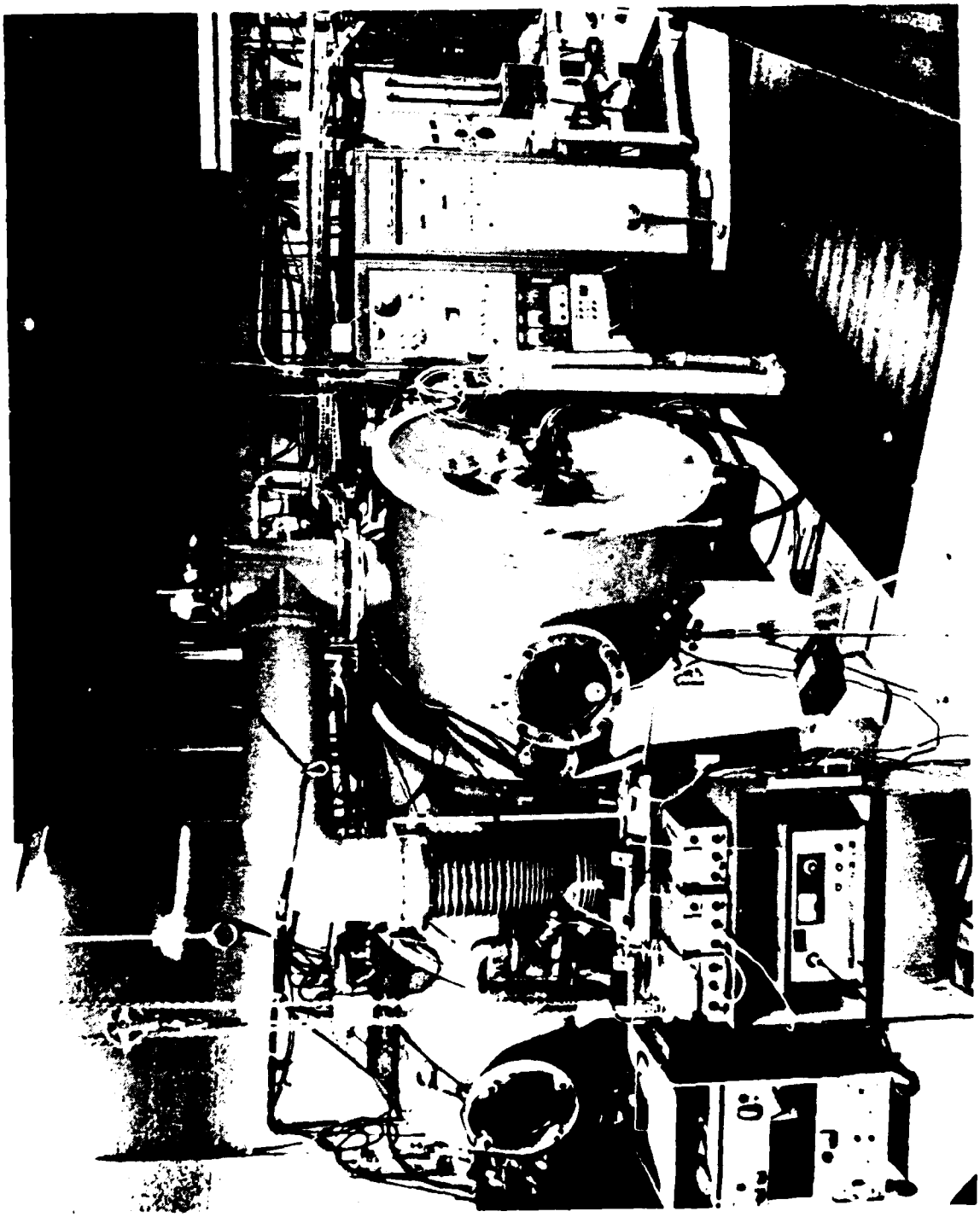

Fig. 3 Photograph of STD Research Corporation's continuous plasma flow HIMHD facility (ca. 1975)

APPENDIX A

AIAA-84-0155

STRONG MHD INTERACTION

S. T. Demetriades and C. D. Maxwell
STD Research Corporation, Arcadia, CA

Presented at
AIAA 22nd Aerospace Sciences Meeting
Reno, Nevada
January 9-12, 1984

AIAA'84

AIAA-84-0155

Strong MHD Interaction

S.T. Demetriades and C.D. Maxwell
STD Research Corp., Arcadia, CA

AIAA 22nd Aerospace Sciences Meeting
January 9-12, 1984/Reno, Nevada

STRONG MHD INTERACTION

S. T. Demetriades* and C. D. Maxwell†

STD Research Corporation
Arcadia, CA 91006

Abstract

Plasma flows with strong magnetohydrodynamic (MHD) interaction are examined in numerical simulations of situations of interest for high performance MHD energy conversion. The importance of flow distortions and nonideal processes associated with strong MHD interaction is shown to be well established experimentally. Strategies for managing these processes are examined in order to extend present MHD performance levels beyond the 0.6 - 0.7 MJ/kg specific energy extraction demonstrated to date in combustion driven generators. The role of the plasma boundary configuration in determining the flow development and the likelihood of the development of the magnetoaerothermal instability is illustrated. Finally, the importance of high magnetic Reynolds number effects are considered for MHD devices capable of high levels of MHD interaction.

Introduction

We consider here effects inherent in high performance magnetohydrodynamic energy conversion devices, particularly those which employ plasma as the working fluid. Five nondimensional parameters characterize the global magnetohydrodynamics in such devices: the Mach number, an MHD interaction parameter defined below, the aspect ratio (L/D), the viscous Reynolds number, Re, and the magnetic Reynolds number, Rm. Numerous local magnetogasdynamic, thermal, kinetic, and electrical nondimensional parameters also govern the local behavior of such devices.

Given practical constraints on magnetic field (1-10 T), length-to-diameter ratio (10 to 1000), and mass density of the plasma (> 0.01 kg/m^3), such devices may have length scales of the order of 0.1 to 100 m. Figs. 1 and 2 give typical values of these constraints and the feasible domain for two MHD accelerator devices. The Mach number will vary from high subsonic for some fossil-fueled devices to $M > 10$ for some explosive devices. The viscous Reynolds number will be of the order 10^6.

While idealized, one-dimensional models of the flow in such devices may be adequate to describe situations in which the interaction between the working fluid and the ponderomotive (Lorentz) forces is weak, more elaborate models must be employed to simulate devices in which the interaction parameters and/or magnetic Reynolds number reach high values. Highly unconventional and three-dimensional flow behavior results from strong interaction between the Lorentz forces and the fluid. This paper reviews the operating regimes of major classes of MHD power generators tested to date, examines unconventional phenomena predicted to occur in such devices, and describes the recent experimental confirmation of the magnetoaerothermal effects predicted by the STD/MHD codes and reported for the first time three years ago at this meeting.

*President and Technical Director, Associate Fellow AIAA
†Vice President and MHD Project Manager, Member AIAA

The STD/MHD Codes

The physical processes which govern MHD device performance are numerous and interdependent, and crucial phenomena may easily be obscured by intuitive, simplified, or decoupled analyses. Many such processes are inherently unsteady, probabilistic, and/or three dimensional.

Comprehensive analytical tools are required for unambiguous interpretation of MHD experimental data and to extend test data to new designs, larger scales, or higher levels of MHD interaction. The STD/MHD codes are constructed from a large collection of modules or subprograms which address various aspects of the MHD problem. Taken together, these codes comprehensively define and solve the MHD problem.

The theoretical foundation for these modules has been laid over the past 25 years by the senior author and his coworkers. The formulations for most of these modules are documented in Ref. [1] and its references, as well as several more recent STD Research Corporation publications (e.g., [2] - [4]).

Post-test simulations of well-diagnosed experiments have never failed to verify the accuracy of the STD/MHD codes within the experimental tolerances of the measured input data [5], [6]. The STD/MHD codes have been shown to be sufficiently sensitive to detect subtle inconsistencies in input data furnished by experimenters. These inconsistencies were confirmed by the experimenters only after they were pointed out to them by STD Research [5]. The STD/MHD codes have been used as engineering tools to design MHD devices, improve the performance of devices designed by others, predict nominal performance, and assess the impact of design changes for a number of new MHD devices. These designs, improvements and predictions have always been proven or verified when the devices were tested [6].

Most importantly, in a number of cases anomalous or unexpected phenomena have emerged from three-dimensional and/or time-dependent simulations with the STD/MHD codes before experimental observations of the phenomena were available. Many of these effects have been verified subsequently, and none have been disproven. For many processes, such as the magnetoaerothermal effect [7], the phenomena involve such complex interactions that it is doubtful that a prediction or complete understanding would have been possible without the physical insight provided by comprehensive numerical simulations and adequate computer graphics.

These codes are available and accessible to all who need to use them.

MHD Performance and MHD Interaction

While the STD/MHD codes have also been validated in many weak-interaction MHD situations, (indeed, with no magnetic field they have been validated as computational fluid mechanics codes), it is at moderate to high levels of MHD interaction that a comprehensive, fully coupled analytical approach is required. Since it is also at high levels of MHD interaction that the performance of MHD devices becomes attractive, simplified treatments have limited usefulness, even for system calculations.

The relationship between performance and MHD interaction is well known. One way of expressing this relationship [8] is that the energy-per-unit-mass, or specific energy, that is added or removed from the plasma flow in MHD devices varies directly as the product of the conversion efficiency η_e and the interaction parameter I_p,

$$P/\dot{m} \propto \eta_e I_p \tag{1}$$

where we have used the symbol P for the electrical power and $\dot{m}$ for the mass flow rate. The proportionality constant in this expression is approximately RT, the product of the gas constant and the temperature of the working fluid. The conversion efficiency is defined by $\eta_e = \vec{J}\cdot\vec{E} \;/\; \vec{J}\cdot(\vec{U}\times\vec{B})$, while the interaction parameter I_p is defined over the length L of an MHD device by the expression

$$I_p = \int_0^L \frac{|\vec{J}\times\vec{B}|}{p}\, dx \tag{2}$$

where p is the static pressure in the flow.

It is noted that other equivalent forms of Eq. (1) may be written. These may involve other measures of performance, such as enthalpy extraction ratio. However, it is not strictly valid to write, as some have done, performance as varying with the interaction parameter I_p alone; to cite an extreme example, high values of I_p may be reached by short-circuiting a generator, but no power is produced. Performance requires interaction and efficiency.

One can also consider two interaction parameters, namely, the ratio of Lorentz force per unit volume to the momentum flux or dynamic pressure, $i_1 = (J_y B/\rho U^2)$, and the ratio of Lorentz force per unit volume to static pressure p, $i_2 = (J_y B/p)$. These, as well as the local magnetic Reynolds number, $r_m = \mu_0 \sigma U$, can be made nondimensional by integrating over a length, L. The nondimensional interaction parameter obtained by integrating i_1 is called the interaction parameter based on velocity, S_u. The nondimensional interaction parameter obtained by integrating i_2 is the interaction parameter based on pressure, I_p, defined above. Rm is the nondimensional magnetic Reynolds number.

It is noted that $i_2 = i_1(c_p/c_v)M^2$, where c_p/c_v is the ratio of specific heats and M is the Mach number. Thus for a given performance level characterized by I_p, S_u will vary inversely as the square of the characteristic Mach number in the device. While I_p correlates performance, S_u correlates flow distortion and behavior [8]. It follows that for two devices with the same performance, expressed in power per unit mass flow, the device with the lower Mach number will exhibit the greater flow distortion.

Figs. 3 and 4 present a map of the characteristic parameters I_p, S_u and Rm for MHD devices using as working fluids combustion products of fossil fuels and solid propellants, explosion products and noble gases, and arc-jet heated nitrogen and argon. The highest levels of interaction were achieved in the arc-jet experiments, which were run both in the generator and accelerator modes [9] - [11]. The highest magnetic Reynolds numbers were obtained in the explosive MHD experiments, which also exhibit the lowest values of S_u because of high Mach numbers.

The Appendix to this paper, taken from [12], derives expressions for the power from an idealized MHD generator with arbitrary magnetic Reynolds number. It is shown that power varies as tanh(Rm/2). For Rm << 1, the power varies as Rm in accordance with textbook formulas for low magnetic Reynolds number MHD. However, for Rm of order unity or greater, power tends toward an asymptotic limit as the hyperbolic tangent tends toward 1. For Rm = 3, power has reached 90% of its asymptotic value. Further increases in conductivity and velocity for the sake of increasing power yield diminishing returns, especially when losses are considered.

The validity and universality of the correlation in Eq. (1) is shown by Fig. 5. The specific energy extraction P/m is plotted versus the product $\eta_e I_p$ for fossil-fueled and solid propellant experiments and designs in the U.S. and elsewhere. These points have all been plotted following determination of these parameters from the experimental data or simulations of proposed devices with the STD/MHD codes. These codes automatically display such parameters as η_e and I_p as well as the extracted electrical power. The experiments span a wide range of length scales (0.5 to 30 m), configurations (linear or disk, square, octagonal, round, etc.), electrical connections (Hall, Faraday, windowframe and external diagonal), and working fluids (toluene, JP-4, coal, natural gas, solid propellants, etc., all at various stoichiometries).

The levels of interaction spanned in Fig. 5 have been subdivided into four regimes based on a qualitative assessment of the degree of MHD flow distortion observed in the simulations of these devices. Because the degree of MHD flow distortion at a given I_p also depends upon the Mach number in each device, these subdivisions are approximate.

Many experiments have been carried out in the low-interaction regime, where the fluid behavior is conventional, i.e. as in ordinary fluid mechanics, with only second-order corrections for MHD effects. The simulation of these experiments with the STD/MHD codes has shown that the second order modifications to friction and heat transfer due to the weak Lorentz forces and ohmic heating alter the conventional duct-flow behavior very slightly. The weak secondary flow pattern arising from the viscous interaction between the flow and the walls (an eight cell pattern in a square duct) may be

disrupted by the weak MHD interactions, which promote nonuniform transverse body forces, but the bulk flow properties are virtually unaffected. The flow field can then be adequately predicted with the methods of conventional gasdynamics merely by accounting for the additional average axial body forces and the bulk ohmic heating of the gas.

The few experiments that have been carried out in the high-interaction regime (see Fig. 5) have shown significant MHD effects on the bulk flow of the plasma, notably flow asymmetry and distortion. These high-interaction experiments include the AVCO Mark V [13], the Viking I tests at the Wright Patterson APL [14], the Bangerter solid propellant experiment at Hercules, Inc. [15], the Pamir I experiment with solid propellant [16], and the AEDC High Performance Demonstration Experiment (HPDE) [17]. In all of these experiments the specific energy extraction reached at least 0.6 MJ/kg. STD Research Corporation has performed extensive simulations of these experiments, especially the AEDC/HPDE, and has shown the influence of these effects in detail, as will be discussed below.

The importance of high-interaction phenomena has been appreciated by many of the experimentalists who have achieved the highest levels of performance. For example, at the conclusion of the Pamir I experiments in the Soviet Union [16] it was noted that,

> "Using an effective solid-fuel plasma generator, specific power output and power density of up to 0.6 MJ/kg and 500 W/cm^3, respectively, was generated. Further increasing these parameters (and accordingly ... the coefficient of enthalpy extraction) can be achieved only if the limiting effect of processes associated with strong interaction are suppressed. The nature of these processes is not yet fully understood, thus it is necessary to continue the study of these phenomena."

In the high and very high interaction regimes, where the nonlinear coupling of the flow field to the Lorentz forces and the ohmic heating will be very strong, the plasma flow will be dominated by MHD effects. This is clearly indicated by the experience obtained by the STD/MHD code simulations as the interaction level and performance increase. This experience will be reviewed in the following section.

High Interaction MHD Phenomena

The successful validation and use of the STD/MHD codes under moderate-to-high levels of MHD interaction have demonstrated that, as the MHD interaction increases, profound changes can take place in the fluid dynamic behavior of the duct. The following unconventional effects are some of those that have been observed in both the computer simulations and the experimental data obtained to date:

(1) Sidewall velocity overshoots. Diminished axial Lorentz forces in the boundary layers on insulating sidewalls permit the sidewall working fluid to accelerate relative to the core fluid [18], [8]. When current is allowed to flow to the sidewalls of a generator, the resulting decrease in Lorentz force over the electrodes can lead to similar velocity overshoots in the electrode boundary layers [19]. In channels of high interaction, neglect of this effect leads to serious errors in determining the blockage at the diffuser entrance and the resulting diffuser performance [8].

(2) Transverse static pressure anomalies. The virtually unavoidable presence of local axial currents promotes spatially nonuniform body forces on the working fluid in the direction perpendicular to both the mean flow and magnetic field directions. In the case in which the average of these transverse body forces is not zero in the cross section, a transverse pressure gradient is sustained [19]. This may occur even in a segmented Faraday device in which the net Hall current is zero.

(3) Transverse asymmetries in the electric field distribution. Secondary flows and the magnetoaerothermal effect redistribute the momentum and energy fields of the working fluid. This is observed in measurements of the transverse voltage profiles of moderate-to-high interaction MHD generators [6].

(4) Transverse asymmetries in the velocity field. Nonuniform Lorentz force distribution in the cross section results in skewed profiles of axial velocity. Such velocity asymmetries are manifested in asymmetric stagnation pressure profile measurements [21].

(5) The magnetoaerothermal effect. This effect causes asymmetric boundary layer deceleration or stall (separation) at the center of the anodes in an MHD generator. Even in segmented Faraday generators or accelerators with significant interaction levels, correct analysis shows that there exist significant Hall currents nonuniformly distributed in the cross section, even at zero integrated Hall current. The nonuniformity in the transverse Lorentz force field caused by these Hall currents drives strong secondary flows (in confined channel flows what goes up must come down; in free jets the jet is permanently deflected; under the right conditions the flow oscillates) [7] and [22]. The secondary flow components on the transverse plane direct hot plasma on the center of the anode walls. This, among other things, constricts the discharge or current paths over the anode (which promotes stronger Hall current gradients and secondary flows), causes a large increase in the local current density, and increases the local interaction (hence the local or not-so-local stall in generators) and the local heat transfer. The cathode boundary layer is also influenced by the magnetoaerothermal effect and may show a tendency to stall further downstream and away from the cathode center in segmented Faraday generators.

Fig. 4 illustrates these effects, especially (1), (3), (4), and (5), on the basis of the STD/MHD code simulations of the AEDC/HPDE Run MI-006-014.

This figure gives a capsule view of the effects of MHD interaction. Because the interaction parameter increases directly with length, the velocity and temperature profiles and current and secondary flow patterns at successive axial stations illustrate the magnitude of MHD flow distortion found at successively higher levels of MHD interaction.

To illustrate how the magnetic field and wall temperature can influence the development of high interaction MHD phenomena, Figs. 7 and 8 show a progression of computations with peak magnetic field increasing from 3 to 5 tesla for the conditions of the AEDC/HPDE Run MI-006-014 (see Fig. 4), except that the electrode wall temperature has been elevated from values of 1050 K maximum to values of 1700 K maximum. The development of the velocity profiles and secondary flows shown in Fig. 7 and the development of the static temperature and transverse current distribution shown in Fig. 8 clearly demonstrate the strengthening of the above effects as magnetic field increases. Equally important is the observation that the strength of the above effects is diminished by the increase in wall temperature, as was shown in Ref. [22]. Hotter walls promote a more uniform conductivity field, which leads to weaker Hall current gradients in the cross section [7].

All of the above effects are now well established experimentally:

(1) Sidewall velocity overshoots have been directly measured by Rankin at Stanford University [23] and more recently by McClaine, et al. at Avco Everett Research Laboratory [24].

(2) Transverse static pressure gradients have been observed in every high interaction experiment in which they have been investigated. Especially severe static pressure anomalies are observed in channels which permit a significant net Hall current to flow (e.g., [16]).

(3) Review of the transverse voltage profile measurements over the past 20 years reveals a qualitatively similar asymmetry in them which is due at least in part to the redistribution of momentum and energy in the cross section by MHD interactions. This asymmetric shape is a characteristic of all of the high-interaction three dimensional simulations performed to date, and comparisons between three dimensional simulations and experimental profiles have yielded very satisfactory agreement [6].

(4) Velocity profiles inferred from exit stagnation pressure profile measurements have been shown to be increasingly unconventional and asymmetric from anode to cathode as MHD interaction increases [21], [24]. While there has been a cautious tendency by the experimenters to look for possible explanations for these asymmetries in conventional effects (e.g., shocks) or errors in experimental technique (e.g., probe interactions) [24], the trends in these measurements are now believed to be sufficiently systematic and consistent with predictions of the analytical models to conclude that these asymmetries represent high interaction MHD phenomena.

(5) The above effects (2) - (5) are closely related to the magnetoaerothermal effect. In fact, they may be thought of as precursors or signatures of an incipient magnetoaerothermal current constriction/anode boundary layer stall. Following 1981 predictions by STD Research Corporation that the magnetoaerothermal effect should be observed in the AEDC/HPDE tests, such a magneotaerothermal effect was clearly observed in Run MI-007-016 of 20 October 1982. The following section describes the AEDC/HPDE simulations and data related to the prediction and subsequent observation of the magnetoaerothermal effect.

The Magnetoaerothermal Effect in the AEDC/HPDE

The most recent and the most convincing confirmation of the importance of the above effects has come in the careful and well-diagnosed AEDC/HPDE tests carried out over the past three years.

Prior to the first runs of the HPDE, the three dimensional simulations carried out for a variety of channels from low to high interaction showed the tendency of the anode boundary layer to be stalled by a current concentration in its center at high interaction. Pretest simulations at the nominal design conditions of the HPDE clearly showed the presence of this behavior. Depending on wall and operating conditions, the effects also appeared in simulations with less than the nominal magnetic field strength of 6 tesla. These results were reported in Refs. [7] and [22].

On the basis of the three-dimensional simulations of the AEDC/HPDE carried out by STD Research Corporation, it was possible to predict in early 1981 that [7],

> "Effects of the kind described above [i.e., the magnetoaerothermal effects] should be visible in some of the machines currently under test. For example, the AEDC/HPDE should exhibit accelerated breakdown and erosion of the center of the anodes in the downstream half of the machine. . ."

The first sign that the predicted high interaction phenomena were present in the HPDE tests was the measurement of unmistakable transverse voltage asymmetries in the MI-006 test series data (1979-1980). While the resolution of these data was then somewhat coarse, the agreement with the predictions of the STD/MHD codes was quite satisfactory [6]. The higher resolution transverse profiles of the later MI-007 test series (1981-1982) amply confirmed the presence of the voltage asymmetries [4].

There is a striking similarity between the asymmetric voltage profiles in the AEDC/HPDE [6] and the profiles at the downstream electrodes in previous high-interaction Faraday generator tests (e.g., the Viking I tests -- see Fig. 32 of Ref. [14]). Some of the data from low-interaction Faraday tests appear to contradict these trends [25]. However, (a) the observed differences between anode and cathode are much smaller in the low-interaction tests than in the high-interaction tests, and (b) the weak interaction data of [25]

was taken in the presence of slag, introducing net Hall currents in the plasma due to current leakage in the slag as well as distortions of the cathode voltages by the "stepping" or "staircase" slag shorting effect [26]. The pressure trace of magnetoaerothermal effects is clear in low-interaction machines, although the voltage drop asymmetry is not as pronounced. One thing can be said with certainty: one needs large scale MHD channels or artificially enhanced MHD interactions (e.g., by artificially increasing the conductivity and/or the magnetic field or dropping the pressure, etc.) to make meaningful, large signal-to-noise, measurements of the magnetoaerothermal effects.

Beginning with the MI-007 series of tests at the HPDE, the stagnation pressure profile data approximately one meter downstream of the channel exit strongly suggested the increasing presence of stall on the anode wall as the magnetic field was increased in successive runs. Fig. 9 shows the simulated development of the stagnation pressure profiles down the channel under the 5 tesla conditions of Figs. 7 and 8. In Fig. 9 the 3 m and 4 m stations have been expanded and cut away to reveal the centerline total pressure profiles which were measured in the MI-007 tests. The (3 and 4 m stations have approximately the same interaction parameter as the MI-007 tests due to the above-noted dependence of interaction parameter on length.) The qualitative similarity between the computed profiles and the measured profiles is quite good.

Run MI-007-016 on 20 October 1982 was carried out with the highest magnetic field in the test series, 3.8 tesla. For the first half of this 7 second run, the electrical performance of the downstream half of the channel was anomalously degraded. Post-test inspection of the channel showed significant erosion and discoloration in a long stripe down the center of the anode wall in the downstream half of the channel, as predicted in 1981. Fig. 10 presents a photograph of this manifestation of the magnetoaerothermal effect.

Significantly, the anomalous electrical behavior in Run MI-007-016 "healed" approximately half way through the run. It is believed that this behavior was connected with the rise in the wall temperature during the test.

Control of Magnetoaerothermal Effects

At high levels of MHD interaction magnetoaerothermal effects promote nonuniformity in the electrical and thermal stresses on the walls. Therefore, in planning duration tests under "commercial conditions", the local conditions on the perimeter must be matched, rather than "average" or "core" conditions. The role of magnetoaerothermal effects in determining ultimate performance at the very high MHD interaction levels indicated by simplified system analyses remains to be investigated experimentally.

Strategies which can control and even exploit the magnetoaerothermal effects have been investigated by STD Research Corporation, [7],[22]:

(1) Hotter wall surface temperatures increase plasma uniformity and diminish the local Hall currents which drive magnetoaerothermal effects.

(2) For channels with the same performance, higher Mach number designs minimize the interaction parameter based on velocity and therefore the strength of the magnetoaerothermal effects.

(3) Controlled application of axial currents though the choice of the electrical connections and load network can allow the designer to "steer" secondary flows and drive magnetoaerothermal effects in beneficial ways.

(4) Application of inlet swirl can have a strong influence on the development of magnetoaerothermal effects.

(5) Alternate electrode configurations and cross sectional geometries can modify the development of body forces which drive magnetoaerothermal effects. Current control techniques whereby current is forced to follow planned paths to the electrodes also fall in this category.

The success of the above strategies will make or break the design of high performance MHD power generators. We have been searching for improvements in the effective uniformity through use of nonrectangular MHD channel cross sections. Preliminary results for a 1000 MW (thermal) design indicate that: (1) optimization of the channel shape and the extent of electrode coverage on the channel perimeter can yield performance within a few percent of the ideal (perfectly uniform) conditions (Figs. 11 and 12), and (2) even in channels with circular cross sections, substantial secondary flows are generated by the transverse MHD body forces in the plasma (Figs. 13 and 14); thus it is likely magnetoaerothermal effects will have to be reckoned with regardless of channel shape.

Conclusions

This paper presents detailed results of the application of the STD/MHD codes to the design or analysis of a number of specific MHD power generator devices that have been built or examined over the years. In addition, it presents the detailed description of a number of more complex (but equally important) MHD phenomena revealed in detail, again for the first time, by the application of the STD/MHD codes to specific devices capable of operating at MHD interaction and magnetic Reynolds number levels approaching the levels expected to be encountered in real (practical, useful, commercial, etc.) MHD generators.

The STD/MHD codes have been validated both by direct simulation of carefully diagnosed experiments and, even more importantly, by their demonstrated capability to predict and interpret previously unsuspected MHD phenomena which are crucially important for the successful operation of MHD generators. The available experimental data range from the low to the moderate-to-high interaction regimes. While the codes have also been exercised in the high-to-very high regimes desirable for full-scale commercial and other high power systems, there is a scarcity of detailed and sufficient data with which to compare the predictions of the codes at such levels of MHD interaction.

Acknowledgement

This work was supported in part under Contract No. F49620-83-C-0115, U.S. Air Force Office of Scientific Research, Directorate of Physical and Geophysical Sciences, Capt. Henry Pugh, Jr., Program Manager and in part under Contract No. DE-AC22-83-PC60576, U.S. Department of Energy, Pittsburgh Energy Technology Center, Dr. Harold Chambers, Program Manager.

References

1. S. T. Demetriades, G. S. Argyropoulos, and C. D. Maxwell, "Progress in Analytical Modeling of MHD Power Generators," Proc. 12th Symposium on Engineering Aspects of Magnetohydrodynamics, Argonne National Laboratory, March 1972
2. S. T. Demetriades, et al., "STD/MHD Code Descriptions for Computer Programs Utilized under Contract AC-01-79-ET15501," STD Research Corporation Final Report, Task 1, Contract No. AC-01-79-15501; Report No. STDR-79-3 prepared for ERDA, Div. Magnetohydrodynamics, DOE/ET/15501-1, January, 1979
3. STD Research Corporation, "STD/MHD Codes, Overview and Catalogue of Some of the STD/MHD Code Families Available to the Public," Report No. STDR-104-79, July 1979
4. S.T. Demetriades, C.D. Maxwell, and D. A. Oliver, "Progress in Analytical Modeling of MHD Power Generators II," Proc. 21st Symposium on Engineering Aspects of Magnetohydrodynamics, Argonne National Laboratory, June 1983
5. A. A. Vetter, C. D. Maxwell, and S. T. Demetriades, "The STD/MHD Codes: Comparison of Analyses with Experiments," AIAA Paper 80-0024, AIAA 18th Aerospace Science Meeting, Pasadena, CA, 14-16 January 1980
6. A. A. Vetter, C. D. Maxwell, T. F. Swean, S. T. Demetriades, D. A. Oliver, and C. D. Bangerter, "The STD/MHD Codes: Comparison of Analyses with Experiments at AEDC/HPDE, Reynolds Metal Co., and Hercules, Inc.," AIAA 19th Aerospace Sciences Meeting, St. Louis, MO, Paper No. AIAA-81-0173, January 1981
7. S. T. Demetriades, D. A. Oliver, T. F. Swean, Jr., and C. D. Maxwell, "On the Magnetoaerothermal Instability," AIAA 19th Aerospace Sciences Meeting, St. Louis, MO, Paper No. AIAA-81-0248, January 1981
8. C. D. Maxwell, S. T. Demetriades, D. A. Oliver, A. A. Vetter, T. F. Swean, Jr., "Scale-up of Advanced MHD Generators," AIAA 18th Aerospace Sciences Meeting, Pasadena, CA, Paper No., AIAA-80-0168, January 1980
9. S.T. Demetriades, "Novel Method of Measurement of Plasma Properties by Momentum-Change Techniques," Phys. Fluids, Vol. 4, No. 12, pp. 1569-1570, Dec. 1961
10. S.T. Demetriades, et al., "Three-Fluid Nonequilibrium Plasma Accelerators (Parts I and II)," Electric Propulsion Development, E. Stuhlinger, Ed. Academic Press, N.Y., 1963 and Paper AIAA-63-047, 1963
11. S.T. Demetriades, "Momentum Transfer to Plasmas by Lorentz Forces," Physico-Chemical Diagnostics of Plasmas (Proceedings of the Fifth Biennial Gas Dynamics Symposium), Northwestern University Press, Evanston, IL, November 1963
12. S.T. Demetriades, J.T. Demetriades, and A.S. Demetriades, "Influence of Magnetic Reynolds Number on Power Generated by an Ideal MHD Device," (to be published), July 1983
13. Avco Everett Research Laboratory, "Detailed Performance Evaluation of the Mark V Self-Excited Rocket Driven MHD Generator," AFAPL-TR-65-112, November 1965
14. R. Kessler, O. K. Sonju, J. Teno, L. Lontai, and D. Meader, "MHD Power Generation (Viking Series) with Hydrocarbon Fuels," AFAPL TR-74-47, Part III, Final Technical Report under Contract F333615-71-C-1456, November 1974
15. C. D. Bangerter, B. D. Hopkins, and T. R. Brogan, "Pulsed Magnetohydrodynamic Program," Final Report on contract F22615-72-C-1394, Technical Report no. AFAPL-TR-76-34, July 1976
16. Ye. P. Velikhov, Yu. M. Volkov, A. V. Zotov, O. G. Matveyenko, and A. A. Yakyushev, "Factors Influencing The Self-Excitation of Pulse Type MHD Generators," Proc. 6th International Conference on Magnetohydrodynamic Electrical Power Generation, Vol. VII, p. 141, Washington D.C., June 1975
17. L. S. Christiansen, G. L. Whitehead, and E. J. Felderman, "Performance Results of a 300 MWth Generator at High Magnetic Field," Paper AIAA-83-0394 presented at the 21st AIAA Aerospace Sciences Meeting, January 1983
18. C. D. Maxwell, E. D. Doss, B. F. Curry, and D.A. Oliver, "Consideration of Three-Dimensional Effects in MHD Power Generators," Proc., 15th Symposium on Engineering Aspects of Magnetohydrodynamics, U. Penn., Philadelphia, p. IX.6.1, 1976
19. C. D. Maxwell, D. M. Markham, S. T. Demetriades, and D. A. Oliver, "Coupled Electrical and Fluid Calculations in the Cross Plane in Linear MHD Generators," Proc., 16th Symposium on Engineering Aspects of Magnetohydrodynamics, U. Pitt., Pittsburgh, p. VII.3.13, May 1977
20. T. F. Swean, D. A. Oliver, C. D. Maxwell and S. T. Demetriades, "Prediction of Transverse Asymmetries in MHD Ducts with Zero Net Hall Current," AIAA J., Vol. 19, No. 5, pp. 651-653, May 1981
21. STD Research Corporation, "Analytical Investigation of Critical MHD Phenomena," DOE/NASA/-0202-1, NASA CR-168079, Annual Report STDR--82-15 under NASA contract DEN3-202, Sept. 1981
22. C. D. Maxwell, T. F. Swean, Jr., A. A. Vetter, R. D. Crouse, D. A. Oliver, C. D. Bangerter, and S. T. Demetriades, "Three-dimensional Effects in Large Scale MHD Generators," AIAA 14th Fluid and Plasma Dynamics Conference, Palo Alto, CA, Paper No. AIAA-81-1231, June 1981
23. R. R. Rankin, "Topical Report on Insulating Wall Boundary Layer in a Faraday MHD Generator," Stanford University Report FE-2341-7, April 1978
24. A. W. McClaine, D. W. Swallom, and R. Kessler, "Performance Characteristics of Subsonic Generators," Proc., 20th Symposium on Engineering Aspects of Magnetohydrodynamics, U.C. Irvine, Irvine, Calif., p. 4.1.1, June 1982
25. R. Kessler and A. Solbes, "Detailed Characterization of MHD Generator Operating Parameters," Proc. 17th Symposium on Engineering Aspects of Magnetohydrodynamics, Stanford U., Stanford, Calif., p. F.4.1, March 1978
26. S. T. Demetriades, D. A. Oliver, and C. D. Maxwell, "Current Transport Mechanisms in the Boundary Regions of MHD Generators," Paper AIAA-80-0249, 18th Aerospace Sciences Meeting, Pasadena, Calif., January, 1980

Appendix
Influence of Magnetic Reynolds Number on Power Generated by an Ideal MHD Device

In this Appendix we derive a simple expression for the power of an ideal, one-dimensional MHD generator that is not restricted by the usual assumption of a very small magnetic Reynolds number. It applies to pulsed MHD generators and, possibly, to other devices. It shows that as the magnetic Reynolds number increases, the power to the load approaches an asymptotic limit.

Consider the MHD problem in a channel of constant cross-section A with components of velocity $\hat{U} = (U_x,0,0)$ and magnetic induction $\hat{B} = (0,0,B_z)$ and continuous electrodes of length a along the x-axis on the y-walls at y = 0 and y = h. There is no externally applied electric potential and the conductivity is scalar and uniform in a region extending from x = 0 to x = a, y = 0 to y = h and z = 0 to z = w. Let a be smaller than the extent of the magnetic field region x_B along the x-axis so that $a << x_B$ and the applied magnetic field B_0 is constant in the region a.

Currently favored expressions for the power generated by a simple, one-dimensional, ideal generator are usually given for the case where the magnetic Reynolds number Rm is much smaller than unity (Rm << 1). These low Rm expressions make no assumption concerning the region of high conductivity in the x-direction, a. In fact, they assume that the magnetic field B is a square function (i.e. they assume $B_z \equiv B_0$ in $0 \le x \le a$ and zero elsewhere). Since for low Rm, $B_z = B_0$, this assumption is valid. For a continuous MHD generator the extent of the high conductivity region can be assumed to be infinite (i.e. σ is high in the region from x = 0 to x = ∞ and only the extent of $\hat{B}$ is limited).

In this analysis we consider the extent of the high conductivity region to be limited to $0 \le x \le a$ and $a < x_B$.

From Ohm's law we obtain, for the given geometry,

$$J_y = \sigma E_y' \tag{3}$$

while E_y' is given by

$$E_y' = E_y - U_x B_z \ . \tag{4}$$

Note that the minus sign in Eq. (4) is a simple consequence of the geometry. Then we obtain

$$J_y = \sigma E_y' = \sigma(E_y - U_x B_z) = -\sigma U_x B_0 \left[\left(\frac{B_z}{B_0}\right) - K_y\right] \ , \tag{5}$$

and the power per unit volume of plasma P delivered to the load (in the generator case) is given by

$$P = \hat{J}\cdot\hat{E} = J_y E_y = -\sigma U_x^2 B_0^2 K_y \left[\left(\frac{B_z}{B_0}\right) - K_y\right] \tag{6a}$$

where

$$E_y \equiv K_y U_x B_0 . \tag{6b}$$

The negative sign convention means that power is removed from the plasma.

The magnetic Reynolds number for the given geometry is given by

$$Rm \equiv \mu_0 \sigma U_x a . \tag{7}$$

To determine the influence of Rm on the total power it is necessary to integrate Eq. (6) over the interaction region, which, because of uniformity of the parameters involved, is equivalent to integration over x in the interval from x = 0 to x = a. Before we attempt this integration note that we can obtain from the Maxwell equations:

$$\nabla\times\hat{B} = \mu_0 \hat{J} \tag{8}$$

and for the purposes of this discussion

$$-\frac{\partial B_z}{\partial x} = \mu_0 J_y \tag{9}$$

where the minus sign is again due to the geometry.

At the same time the familiar induction equation can be rederived for this special case as follows: From Eq. (9), by differentiation we obtain

$$\frac{\partial J_y}{\partial x} = -\frac{1}{\mu_0}\frac{\partial^2 B_z}{\partial x^2} \tag{10}$$

and, also by differentiation, from Eqs. (3) and (4) we obtain

$$\frac{\partial J_y}{\partial x} = \sigma\left(\frac{\partial E_y}{\partial x} - U_x\frac{\partial B_z}{\partial x} - B_z\frac{\partial U_x}{\partial x}\right) . \tag{11}$$

Since we have assumed that E_y and U_x remain constant with x for the purposes of this approximation, we obtain

$$U_x\frac{\partial B_z}{\partial x} = \frac{1}{\mu_0\sigma}\frac{\partial^2 B_z}{\partial x^2} \ . \tag{12}$$

This partial differential equation has solutions of the form

$$B_z = B_0 K_y - A_1 e^{Rmx/a} \ . \tag{13}$$

Note that Eq. (13) yields

$$\frac{\partial B_z}{\partial x} = -A_1\left(\frac{Rm}{a}\right)e^{Rmx/a} \tag{14}$$

and

$$\frac{\partial^2 B_z}{\partial x^2} = -A_1\left(\frac{Rm}{a}\right)^2 e^{Rmx/a} \tag{15}$$

Note that from Eqs. (12), (14) and (15) we obtain

$$-U_x\cdot A_1\left(\frac{Rm}{a}\right)e^{Rmx/a} = \frac{1}{\mu_0\sigma}\cdot A_1\left(\frac{Rm}{a}\right)^2 e^{Rmx/a} \tag{16}$$

i.e. Eq. (13) satisfies Eq. (12).

Let the boundary conditions be

$$B_z(0) \equiv B^- \tag{17a}$$

and

$$B_z(a) \equiv B^+ \ . \tag{17b}$$

Then observe that Eq. (9) gives

$$\int_0^a J_y\,dx = \frac{I}{w} = -\mu_0^{-1}\left(B_z^+ - B_z^-\right) \tag{18}$$

where I is the current delivered to the load which in terms of Eq. (5) becomes

$$\frac{I}{w} = -\int_0^a \sigma U_x B_0 \left[\left(\frac{B_z}{B_0}\right) - K_y\right]dx \quad . \qquad (19)$$

In the limit in which we have I = 0, the magnetic field must be equal to the applied magnetic field, $\therefore B_z = B_0$. This is equivalent to demanding that the average of the edge fields be equal to the applied magnetic field, B_0, therefore we have

$$\frac{B_z^+ + B_z^-}{2} = B_0 \qquad (20)$$

Another way of stating Eq. (20) is to say that the induced magnetic field immediately in front of the plasma must exactly oppose the corresponding induced magnetic field at the trailing edge of the plasma or div B = 0.

We can now proceed to solve for the constant A_1. From Eq. (13) we obtain at x = 0

$$B_z^- = B_0 K_y - A_1 \qquad (21a)$$

and at x = a

$$B_z^+ = B_0 K_y - A_1 e^{Rm} \quad . \qquad (21b)$$

Therefore, from Eqs. (20) and (21) we obtain:

$$2B_0 K_y - A_1(1 + e^{Rm}) = 2B_0 \qquad (22)$$

and

$$A_1 = -\frac{2B_0(1 - K_y)}{(1 + e^{Rm})} \quad . \qquad (23)$$

Note also from Eq. (18) we obtain

$$B_z^+ - B_z^- = -A_1(e^{Rm}-1)$$

$$= -\mu_0 \frac{I}{w} = \frac{2B_0(1-K_y)(e^{Rm}-1)}{(e^{Rm}+1)} \quad ,(23a)$$

and thus we can obtain an expression for the total current given by:

$$I/w = -(2B_0/\mu_0)(1-K_y)(e^{Rm}-1)/(e^{Rm}+1) \, . \qquad (23b)$$

Finally, from Eqs. (13) and (23) we obtain

$$B_z = B_0 K_y + \frac{2B_0(1-K_y)}{(1+e^{Rm})} e^{Rmx/a} \quad . \qquad (24)$$

Inserting Eq. (24) in Eq. (5) we obtain

$$J_y = -\frac{2B_0 \sigma U_x (1-K_y) \cdot e^{Rmx/a}}{(1+e^{Rm})} \qquad (25)$$

By differentiation of Eq. (24) we obtain

$$\frac{\partial B_z}{\partial x} = \frac{2B_0(1-K_y)}{(1+e^{Rm})} \cdot \frac{Rm}{a} \cdot e^{Rmx/a} \qquad (26)$$

Therefore, inserting Eqs. (25) and (26) in Eq. (9), we obtain

$$-\frac{\mu_0 \sigma U_x a}{a} = -\mu \sigma U_x \quad , \text{an identity.} \qquad (27)$$

Therefore equations (24) and (25) also satisfy the differential equation for the current density, Eq. (9).

We are now ready to integrate Eqs. (6) and/or (19) to obtain the power as a function of Rm.

Since the electric field in the plasma due to the load is constant, we can write, for the voltage across the load V_L,

$$V_L = E_y h = K_y U_x B_0 h \qquad (28)$$

We observe that the quantity $[(B_z/B_0) - K_y]$, where only the first term is variable, appears in the integrand of both Eqs. (6) and (19) when they are integrated. Let us therefore obtain the integral of this quantity. From Eq. (24)

$$\int_0^a \left[\left(\frac{B_z}{B_0}\right) - K_y\right]dx = \frac{1}{B_0} \int_0^a (B_z - B_0 K_y)dx$$

$$= \frac{1}{B_0} \int_0^a \left[B_0 K_y + \frac{2B_0(1-K_y)}{(1+e^{Rm})} e^{Rmx/a} - B_0 K_y\right]dx$$

$$= \frac{a}{Rm \cdot B_0} \int_0^{Rm} \frac{2B_0(1-K_y)}{(1+e^{Rm})} e^{Rmx/a} \, d\left(\frac{Rm}{a}x\right)$$

$$= \frac{a}{Rm \cdot B_0} \left[\frac{2B_0(1+K_y)e^{Rm} - 2B_0(1-K_y)}{(1+e^{Rm})}\right]$$

$$= \frac{2B_0 a}{Rm \cdot B_0}(1-K_y)\left[\frac{e^{Rm}-1}{e^{Rm}+1}\right] = \frac{2a(1-K_y)}{Rm} \tanh(Rm/2) \qquad (29)$$

Note that this takes care of the integration w.r.t. x only.

Substituting Eq. (29) in the integral over volume of Eq. (6) we obtain for the total power to the load, P_ℓ,

$$P_\ell = \int_0^{a,w,h} P dV$$

$$= -\sigma U_x^2 B_0^2 K_y \cdot \frac{2a(1-K_y)}{\mu_0 \sigma U_x a} \cdot wh \cdot \tanh(Rm/2)$$

$$= -4\left(\frac{B_0^2}{2\mu_0}\right) U_x K_y (1-K_y) \cdot wh \cdot \tanh(Rm/2) \qquad (30)$$

The quantity wh appears when the uniform w.r.t. y and z integrand is integrated w.r.t. y and z and evaluated at y = h and z = w.

We can write Eq. (30) as the power to the load per unit cross-sectional area of the generator channel, A = wh, as

$$P_\ell/A = -4\left(\frac{B_0^2}{2\mu_0}\right) U_x K_y (1 - K_y) \tanh(Rm/2) \qquad (31)$$

Note that since $\tanh(Rm/2) \to 1$ as $Rm \to \infty$, the power obtained from a high magnetic Reynolds number device (e.g. one with very high conductivity) will reach the limit

$$P_\ell/A = -4\left(B_0^2/2\mu_0\right) U_x K_y \left(1-K_y\right) \quad (32)$$

Note that, since already at $Rm = 3$ $\tanh(Rm/2) > 0.9$, for $U = 10^4$ m/sec and $a = 1$ m, we obtain $\sigma = 239$ mho /m. Therefore there is an optimum conductivity for each pulsed MHD generator given by $\sigma \cong 3/\mu_0 Ua$. This expression can be derived by reasoning that operation at a higher magnetic Reynolds number is not required especially since other losses or costs can only increase as Rm is increased. A mindless quest for ever higher conductivity is not necessary.

It is now appropriate to note that Eqs. (30) and (31) both approach zero as $Rm \to 0$. In other words, the power to the load vanishes as $Rm \to 0$. All other expressions are well-behaved also. For example as $Rm \to 0$, Eq. (24) yields

$$B_z = B_0 K_y + \frac{2B_0(1-K_y)\cdot 1}{1+1} \quad (33)$$

$$\therefore \quad B_z = B_0 \ .$$

Eq. (25), for $Rm \to 0$ yields

$$J_y = -B_0 \sigma U_x \left(1-K_y\right) \quad (34)$$

Eqs. (33) and (34) are both the low magnetic Reynolds numbers approximations which yield

$$\left(P_\ell/A\right)_{\text{low Rm}} = -\sigma B_0^2 U_x^2 K_y \left(1-K_y\right) a \quad (35)$$

$$= -\left(\frac{B_0^2}{\mu_0}\right) U_x R_m K_y \left(1-K_y\right) \quad (36)$$

Note that from Eq. (36) we can derive the expression for power to the load per unit volume of plasma in the generator given by

$$\left(P_\ell/V\right)_{\text{low Rm}} = -\sigma B_0^2 U_x^2 K_y \left(1-K_y\right) \quad (37)$$

Equation (37) is the source of some confusion when used for high Rm.

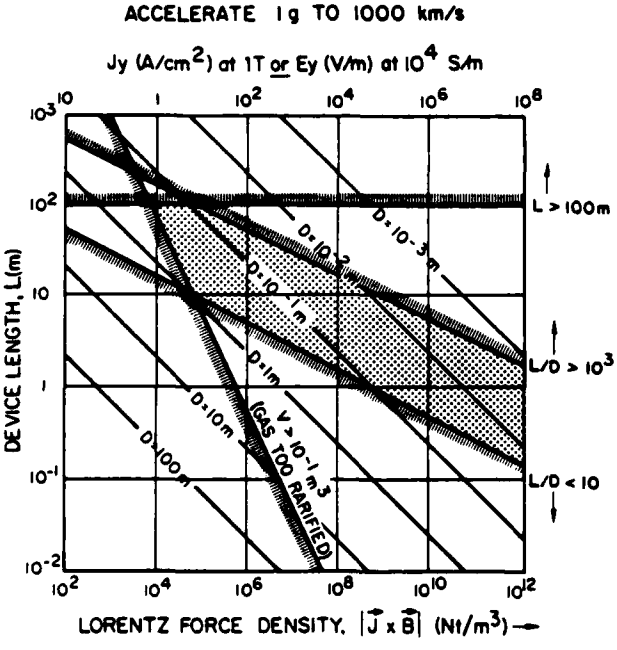

Fig. 1. Feasible domain to accelerate 1 g mass to 100 km/s by application of the Lorentz force in an imposed magnetic field of 1 T in a linear MHD device of length L, diameter D, and volume V. As Lorentz force increases, device scale must decrease for acceptable aspect ratios and mass densities.

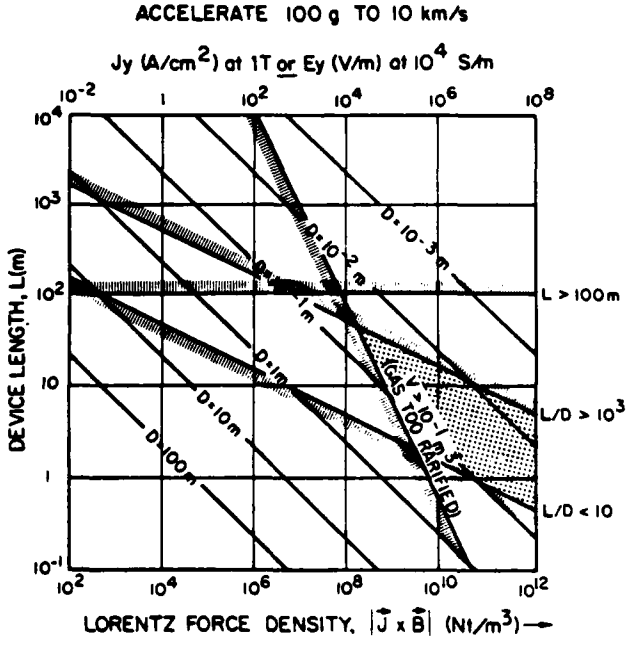

Fig. 2. Feasible domain to accelerate 100 g mass to 10 km/s by application of the Lorentz force in an imposed magnetic field of 1 T in a linear MHD device.

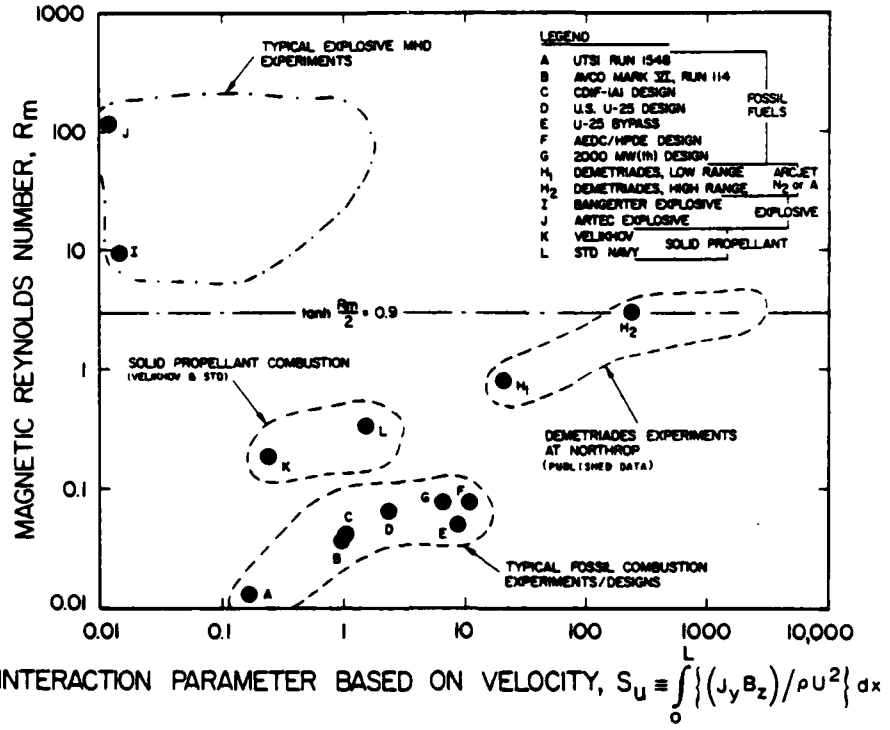

Fig. 3. Map of the magnetic Reynolds number and interaction parameter based on velocity for some significant MHD generator experiments and designs using as working fluids (a) fossil fuel combustion products, (b) solid propellant combustion products, (c) explosion products and noble-gas driver gas, and (d) nitrogen or argon arc-jet plasma.

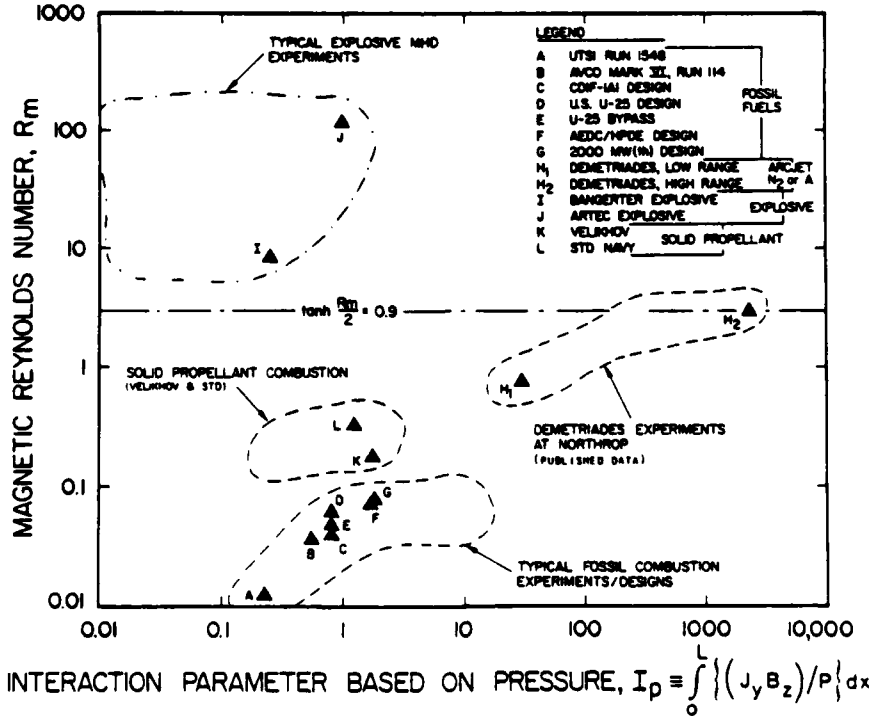

Fig. 4. Map of the magnetic Reynolds number and interaction parameter based on pressure for the same MHD generator experiments and designs given in Fig. 3.

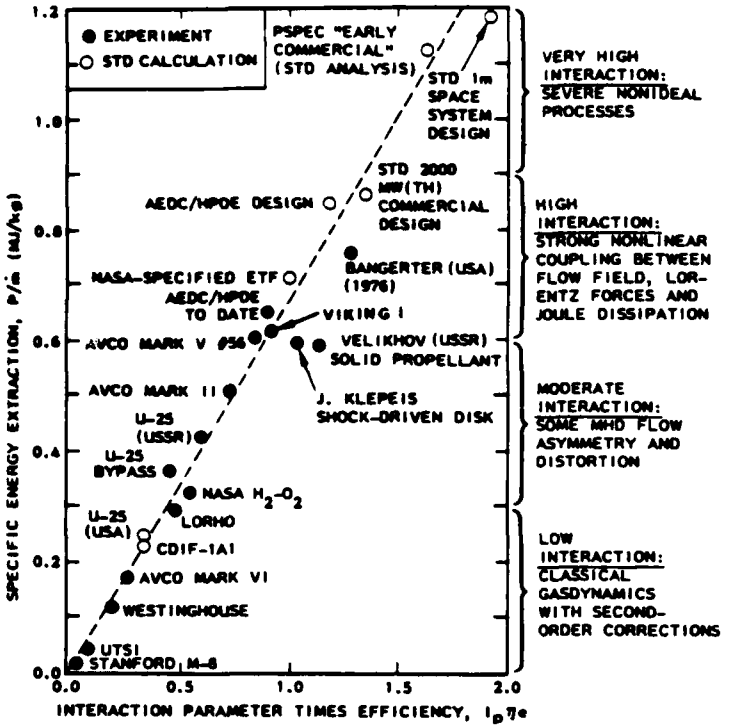

Fig. 5. Interaction levels and specific energy extraction of major MHD power generation experiments and designs in the U.S.A. and the U.S.S.R. Solid points indicate experimental test data. Interaction regimes are arbitrarily divided on the basis of the degree of MHD flow distortion in the STD calculations.

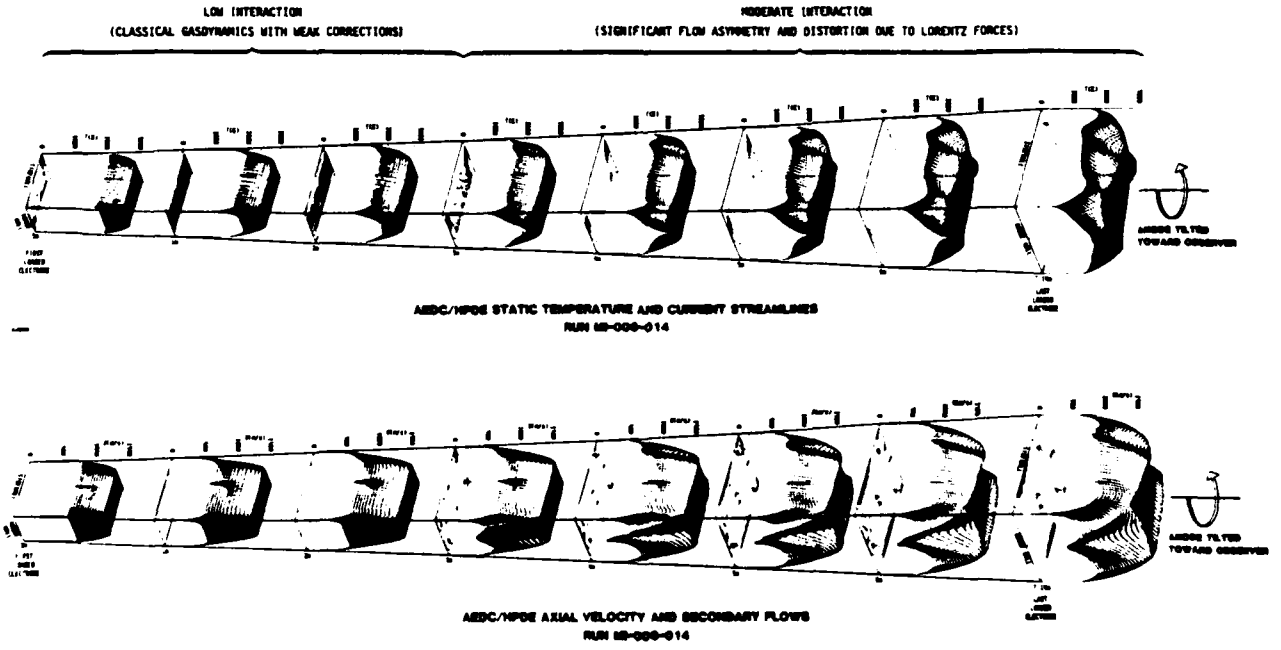

Fig. 6. Development of velocity, temperatures and current under conditions of AEDC/HPDE Run MI-006-014.

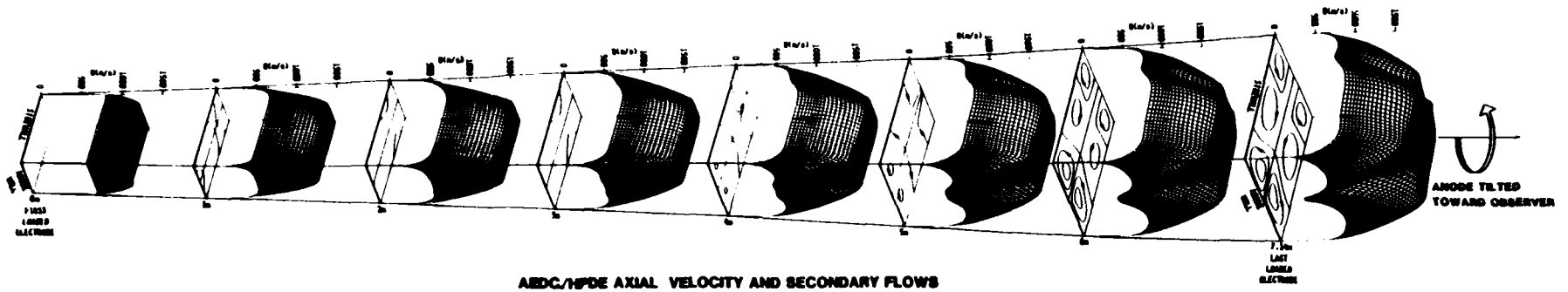

AEDC/HPDE AXIAL VELOCITY AND SECONDARY FLOWS
(a) B_{MAX} = 3T

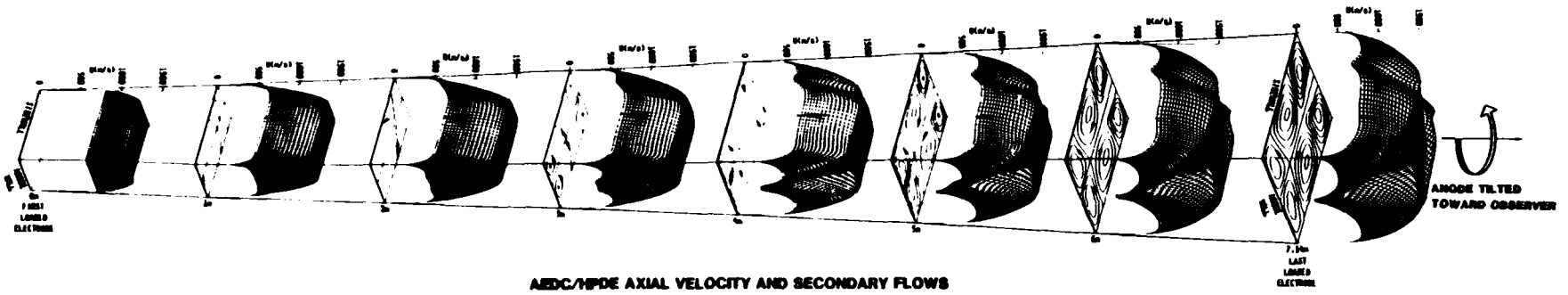

AEDC/HPDE AXIAL VELOCITY AND SECONDARY FLOWS
(b) B_{MAX} = 4T

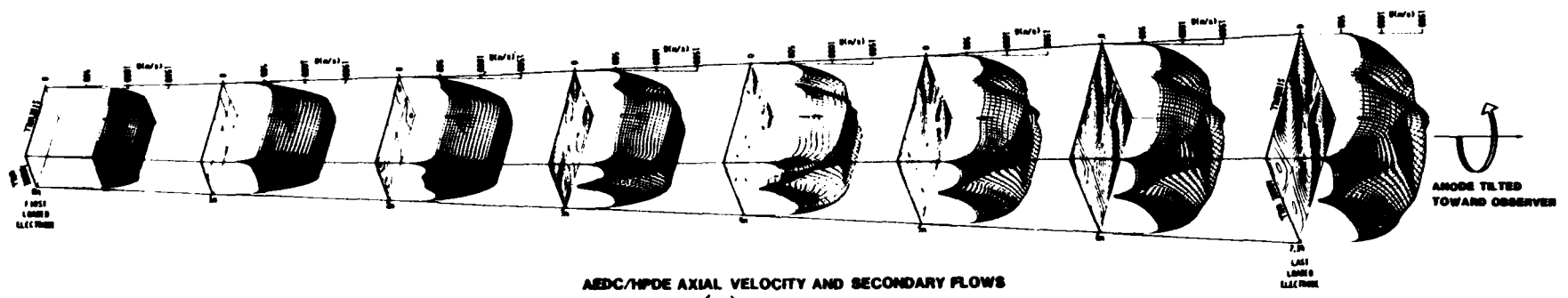

AEDC/HPDE AXIAL VELOCITY AND SECONDARY FLOWS
(c) B_{MAX} = 5T

Fig. 7. Axial velocity and secondary flows in the AEDC/HPDE with hot electrode walls (Tw,max = 1700 K) and peak magnetic induction in the channel of (a) 3 T, (b) 4 T, and (c) 5 T.

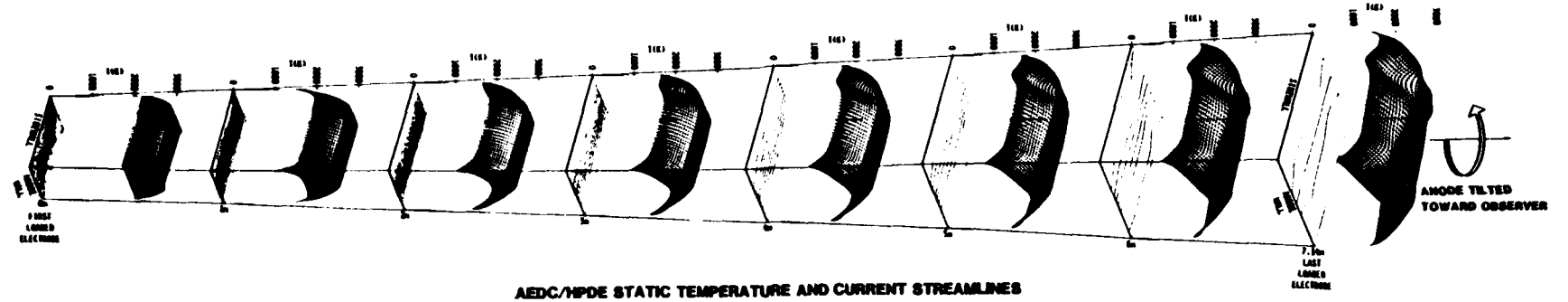

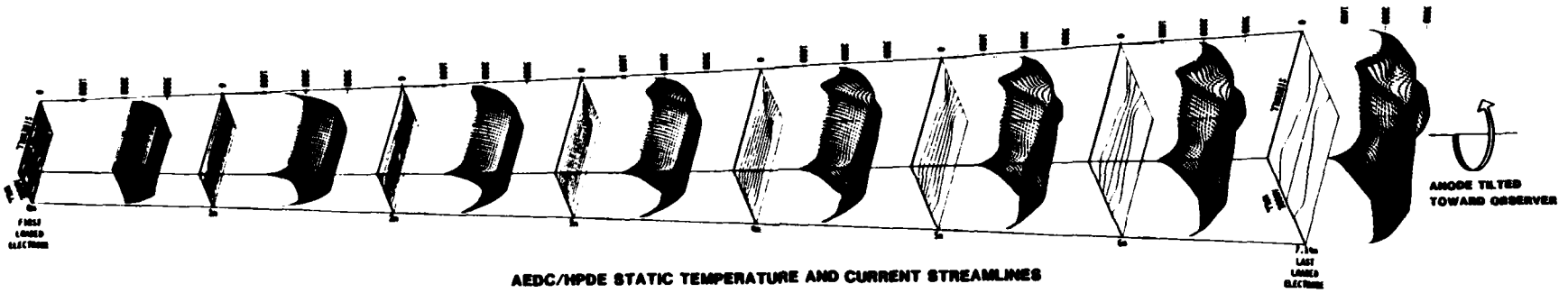

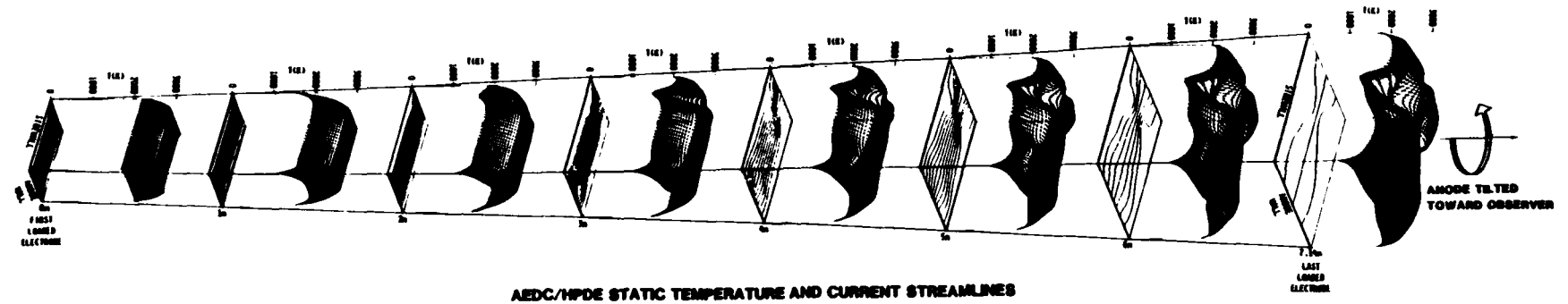

Fig. 8. Static temperature and transverse current distributions in the AEDC/HPDE with hot electrode walls (Tw,max = 1700 K) and peak magnetic induction in the channel of (a) 3 T, (b) 4 T, and (c) 5 T.

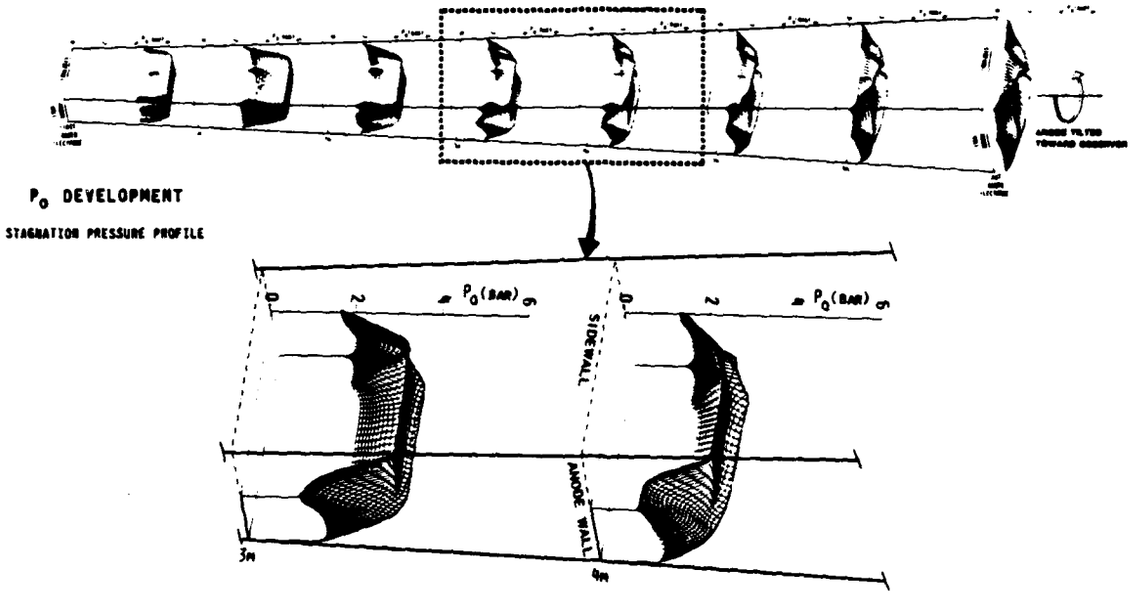

Fig. 9. Development of the stagnation pressure profiles in the 5 tesla AEDC/HPDE simulations of Figs. 7(c) and 8(c).

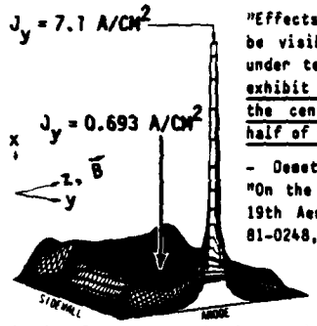

Fig. 8a. Transverse current distribution at 4 meters for conditions similar to those of Table I but with an inlet velocity of 1277 m/sec, a maximum applied magnetic field strength of 3.25 Tesla, and an electrode surface temperature of 750 K. Electrothermal constriction of the magnetoacrothermally induced anode current concentration is clearly in evidence. Maximum total current density in the anode constriction is 15 A/cm^2.

"Effects of the kind described above should be visible in some of the machines currently under test. For example, the AEDC/HPDE should exhibit accelerated breakdown and erosion of the center of the anodes in the downstream half of the machine . . . "

- Desetriades, Oliver, Swean, and Maxwell, "On the Magnetoacrothermal Instability," AIAA 19th Aerospace Sciences Meeting, Paper AIAA-81-0248, p. 6, January 1981.

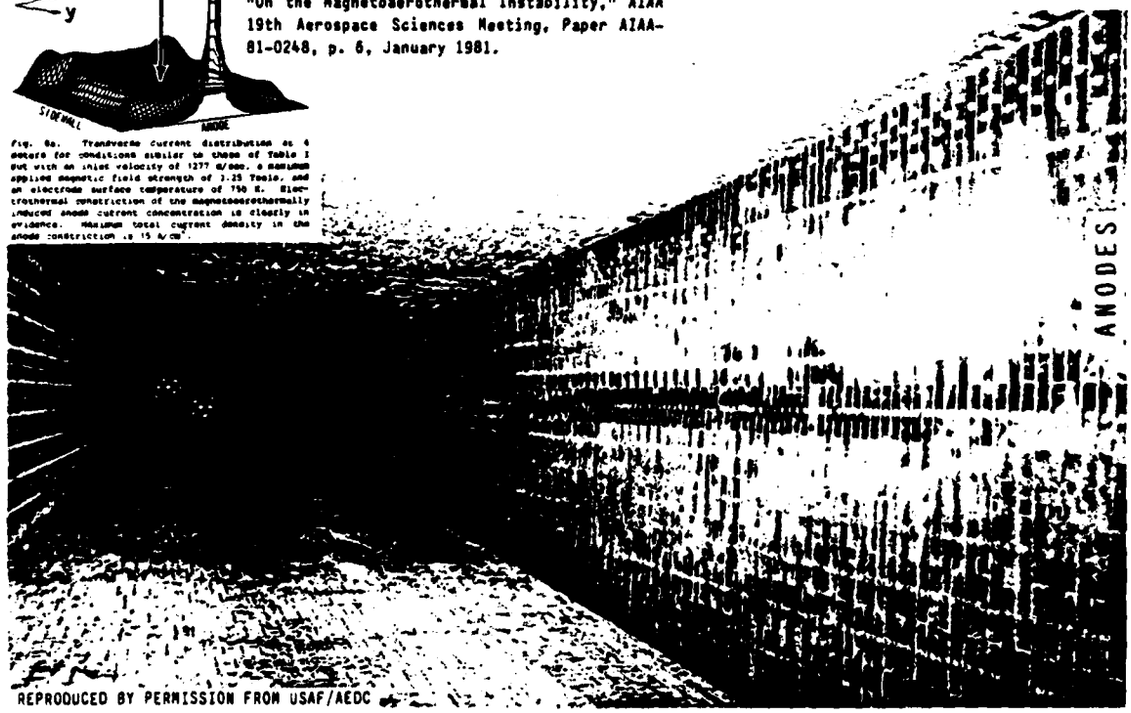

Fig. 10. Interior view of the AEDC/HPDE Channel after Run MI-007-016 of 20 October 1982 showing discoloration to center of anodes between anodes no. 176 and 356. (Anodes receive electrons from the plasma; AEDC designates these electrodes cathodes because they inject electrons into the load.)

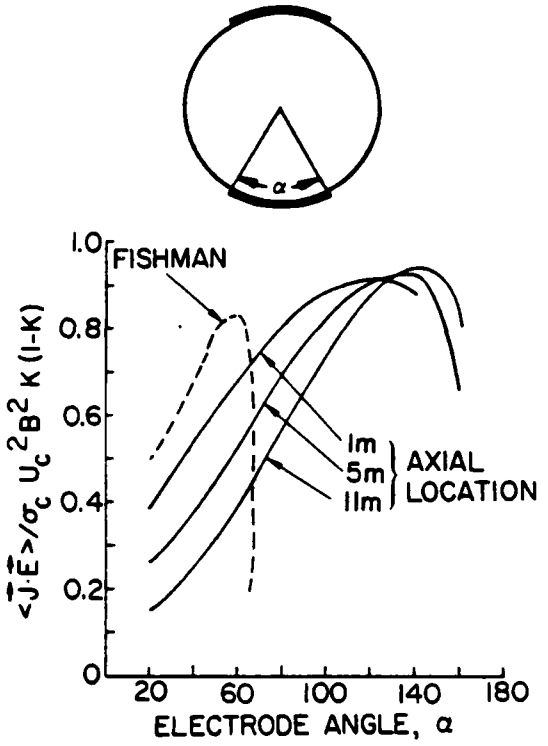

Fig. 11. Total power density relative to the core power density at three stations in a 1000 MW (thermal input) coal-fired MHD generator with circular cross section, as a function of the angle subtended by the electrodes. Also shown (dashed) are the idealized, constant property results of F.J. Fishman, J. Advan. Energy Conv., 4:223-236 (1964).

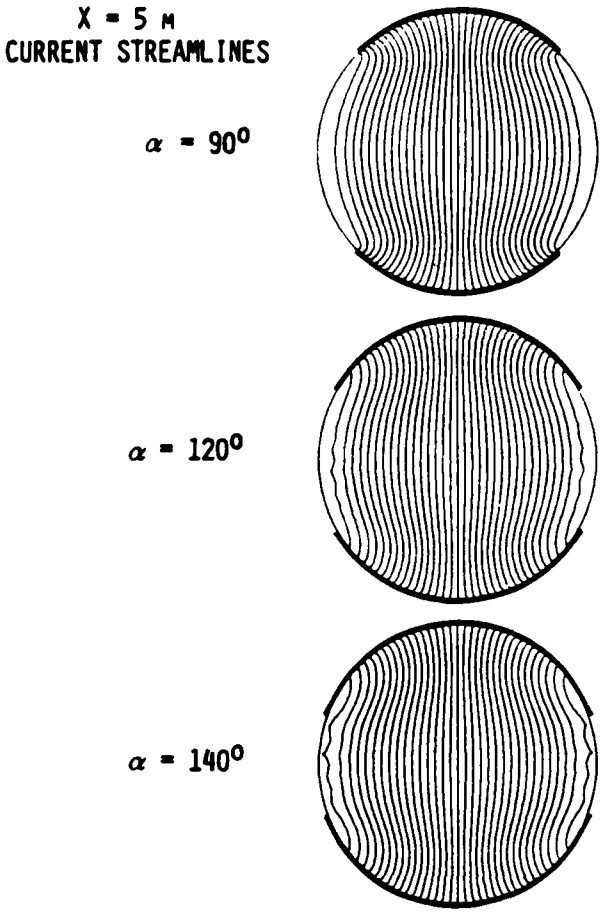

Fig. 12. Current streamlines in the cross section for representative cases from Fig. 11.

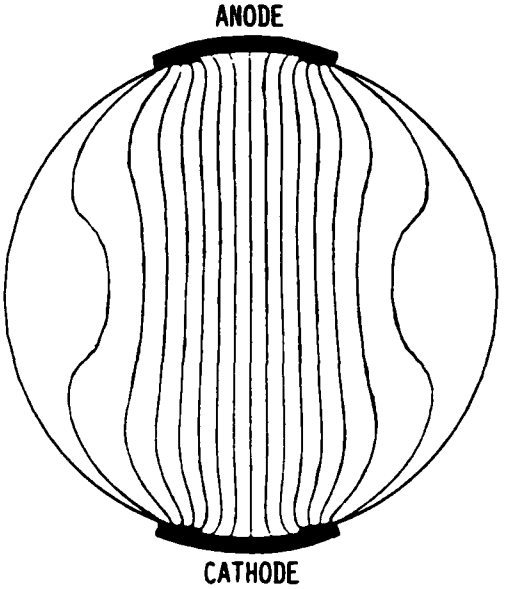

Fig. 13. Current Streamlines in the cross section at the 5 m station in Fig. 11 for an electrode subtended angle of 40°. Peak transverse current density 0.5 A/cm^2.

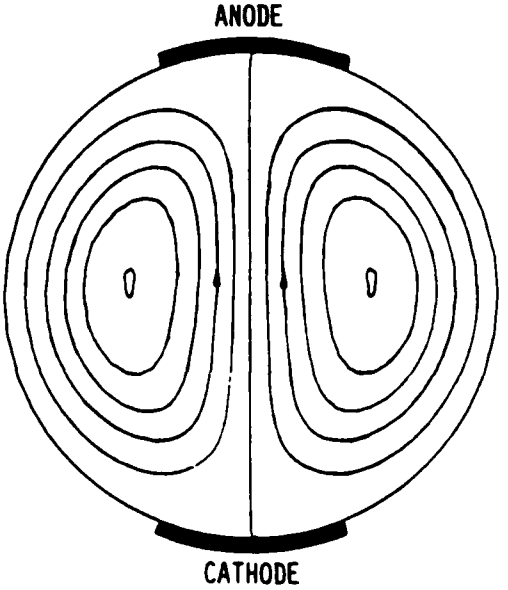

Fig. 14. Streamlines of the secondary flow velocity corresponding to Fig. 13. Peak transverse velocity components are 9% of the mean axial velocity.

APPENDIX B

EXPERIMENTAL MAGNETOGASDYNAMIC ENGINE FOR ARGON, NITROGEN AND AIR

Sterge T. Demetriades

Presented at
2nd Symposium on Engineering Aspects of Magnetohydrodynamics
University of Pennsylvania
9-10 March 1961

STD RESEARCH CORPORATION

Engineering Aspects of Magnetohydrodynamics

EDITED BY
CLIFFORD MANNAL

Experimental Magnetogasdynamic Engine for Argon, Nitrogen, and Air*

STERGE T. DEMETRIADES†

Enthusiasm arises from pride, hope, presumption and a warm imagination together with ignorance. —David Hume

IN LAST year's paper[1] I considered the role of magnetogasdynamics in space propulsion, in general, and orbital propulsion, in particular, and presented the results of studies of a particular space system PROFAC[2]–[4] for which magnetogasdynamic (MGD) propulsion appears to be ideally suited.[2],[3],[5] While presenting that paper I also summarized theoretical results on the dissipative inlet[6]–[8] and the cryopump[5]–[10] required for accumulation of atmospheric gases during acceleration to orbit or in low-altitude orbit. On the basis of previous drag estimates[11]–[13] for powered flight in the upper atmosphere, I gave thrust, specific impulse, and power requirements.[2],[3],[5]–[7],[9] I concluded that if equivalent exhaust velocities of approximately 1.4×10^4 m/sec (i.e., a specific impulse of 1400 kgf-sec/kgm) can be obtained with air or nitrogen at propulsion efficiencies of 20% or better, an order-of-magnitude reduction in size and cost of space transportation systems can be brought about by the application of these electrical engines for air to orbital and space propulsion in conjunction with the PROFAC system.

Theoretical foundations for a continuous MGD engine for atmospheric gases to meet these requirements, special experimental methods and facilities for testing it, and a discussion of MGD acceleration of gases for many other applications (*e.g.*,

*This study was supported by the Northrop Corporation, Hawthorne California.

†Head, Space Propulsion and Power Laboratory, Astro Sciences Group, Norair Division, Northrop Corporation, Hawthorne, California.

orbital or reentry wind tunnel) were presented elsewhere.[3] The first experimental results and the advantages of the continuous MGD engine for air over conventional electrostatic (ion) propulsion devices using air or its constituents, in the required impulse spectrum, were given in more recent publications.[7],[9],[14] Although orbital air-breathing electrical propulsion provided the motivation for this work, many other applications are possible. In this paper I will discuss the experiments in greater detail.

SOME EXPRESSIONS OF INTEREST

The total thrust of a rocket engine Θ_{tr} (exit indicated by subscript 4) which uses a plasma generator followed by MGD thrust augmentation, but without a nozzle after the MGD driver, is given by the sum of the thrust of the plasma generator Θ_{pg} (exit indicated by subscript 2) and the thrust Θ of the MGD driver (exit indicated by subscript 4), i.e.,

$$\Theta_{tr} = \dot{m} U_4 + P_4 A_4 - P_1 A_4 = \{\dot{m} U_2 + P_2 A_2 - P_1 A_4\} + \{\dot{m} (U_4 - U_2) + P_4 A_4 - P_2 A_2\} = \Theta_{pg} + \Theta. \quad (1)$$

The ideal thrust of a rectangular crossed-field MGD driver, without inlet or other losses or cross-sectional area changes and without a nozzle or end effects, is equal to the reaction on the coils, i.e.,

$$\Theta = \dot{m} (U_4 - U_2) + (P_4 A_4 - P_2 A_2) = A\sigma \left(E_o L - B_o \int_0^L U_x \, dx \right) B_o = h I B_o, \quad (2)$$

where L is the length of the driver (along x), A is the cross-sectional area (constant along x), E_o is the electric field (constant along x), B_o is the magnetic induction or flux density [which undergoes a negligible change along x in (U_1, B_2, E_3)-dimensional flow[7],[9]], σ is the conductivity, h is the height of the driver (electrode gap), and I is the total current. Note that as B_o increases, the current density J, given by

$$J = \sigma (E_o - B_o U_x) \qquad \text{amp/m}^2, \quad (3)$$

decreases, and may become zero at a critical value B_{oc} and a given length x. Although the integral of Eq. (2) can be computed by obtaining U_x as a function of x, by techniques given elsewhere,[7] its computation is not required to estimate the

thrust of an MGD driver since the current density or total current can be measured directly or considered as the main parameter.[3] Equations (2) and (3) reveal that the thrust of an MGD driver may reach a maximum as B increases provided the current decreases at the appropriate rate. Equations (2) and (3) also reveal the reason why I prefer the term MGD driver or engine rather than accelerator: The MGD engine can produce thrust (due to a pressure rise) without actually accelerating the stream.

From the above it is clear that in order to obtain a specific impulse of 1400 kgf-sec/kgm (= lbf-sec/lbm) with a flow rate of 10^{-3} kgm/sec, a thrust of 1.4 kgf (13.7 newtons or 3.09 lbf) is required. This corresponds to an equivalent exhaust velocity of 1.37×10^4 m/sec. Assuming that the electrode gap is 4.0×10^{-2} m and the magnetic flux density is 0.2 weber/m^2, the required total current is 1720 amp. Therefore, the problem of producing a sufficiently high specific impulse reduces to one of passing a sufficiently high current between the electrodes at the magnetic fields; flow rates and densities are also involved.[3],[7],[9],[14] This raises a question concerning how much of the energy fed into the stream goes into compression and acceleration (i.e., Lorentz forces or thrust) and how much into other processes, such as dissociation and ionization, thermal losses, etc. To estimate the lumped losses it is necessary to compute the engine propulsion efficiency.

The propulsion efficiency f_r of an electrical rocket is given by

$$f_r = \Theta_{tr}^2 / 2\dot{m} P_{tr}, \quad (4)$$

where $\dot{m}$ is the exhaust mass flow rate and P_{tr} is the total electrical power consumed by the engine. The propulsion efficiency of an electrical ramjet (or of the MGD driver excluding the plasma generator) is given by

$$f = \frac{\Theta^2}{2\dot{m} P_t} + \frac{\Theta U_2}{P_t}, \quad (5)$$

where U_2 is the inlet velocity (or the velocity at the exit of the plasma generator) and P_t is the total electrical power put into the MGD driver including the magnet power and the electrode power. To obtain the propulsion efficiency of the MGD driver or "afterburner" it is necessary to measure the parameters Θ, U_2, $\dot{m}$, and P_t without ambiguity.

EXPERIMENTAL EQUIPMENT

An electromagnet capable of up to 12,000 gauss continuously, or up to 15,000 gauss for short periods, with a gap of approximately 1 in., was mounted on a balance. The balance was enclosed in a vacuum tank where the pressure was maintained at approximately 2000 μ while an argon, nitrogen, or air plasma jet from an arc source was exhausting in it. The plasma jet was directed between the pole pieces of the magnet. The externally applied electric current (or field) in the MGD driver was provided by a pair of tungsten electrodes powered by a battery bank or a set of motor generators. The electrodes were an integral part of the magnet-balance system and the influence of all leads and other lines on the balance was compensated or eliminated. "Frictionless" mercury pots were used to connect the electrodes to the rigid power lines. The balance-magnet-electrode assembly was approximately 1 in., and the pieces and electrodes were approximately 6 in., from the end of the plasma jet nozzle. The electrodes could be adjusted so that they barely touched the free jet of plasma which had a diameter of approximately 1 in. The reaction of the balance was registered by strain gauges. Figure 1 is a schematic of the experimental apparatus. Figure 2 is a partial view of the vacuum tank and the instrumentation and control console. Figure 3 is a view of the balance MGD driver assembly in the vacuum tank with the door open.

The partially ionized plasma flows past the two poles of the magnet (left and right of the MGD section) placed between the

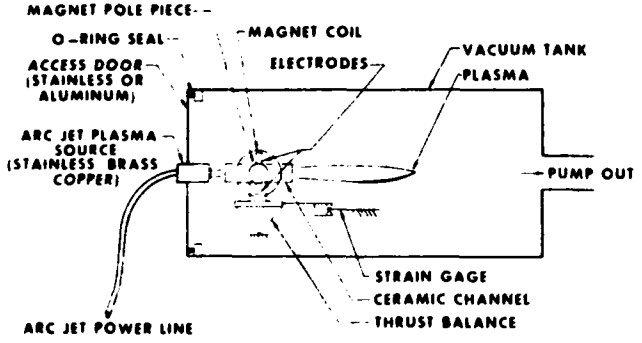

Fig. 1. Schematic diagram of MGD driver balance and vacuum tank system

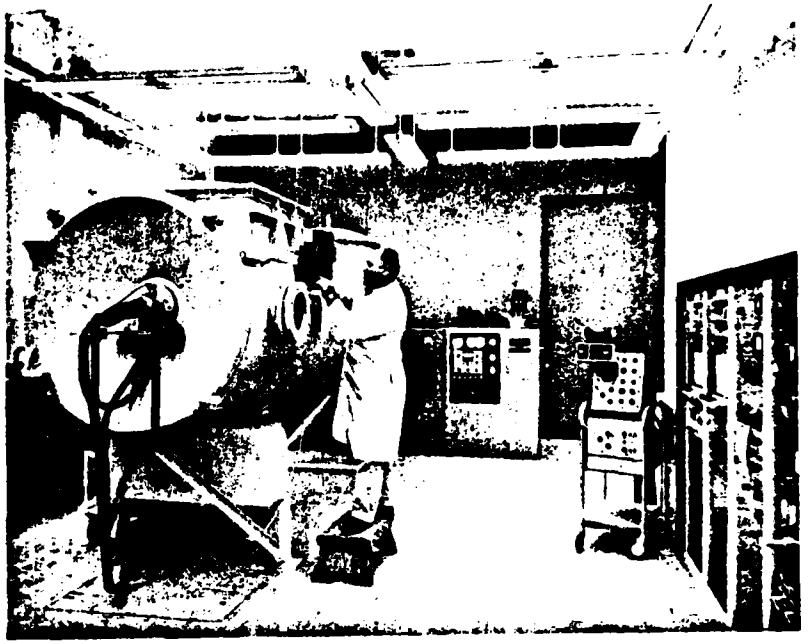

Fig. 2. View of vacuum tank and instrumentation and control console

cathode and anode (top and bottom of the section, respectively). Thus the ionized gas stream conducts an applied electric current perpendicular to both the velocity and the magnetic induction. By choosing the appropriate magnet polarity, the Lorentz force due to the interaction of the current through the gas and the magnetic induction can be made to accelerate the gas down the channel and to increase the exit pressure. The entire assembly, including an inlet to the MGD section, the MGD section or channel itself, and an exit nozzle, is called the MGD driver. Figure 4 is a rear view of the MGD driver or engine mounted on the balance inside the vacuum tank.

In order to isolate the MGD effect from the thermal acceleration effect (due to the heating of the plasma by the current flowing between the two electrodes and subsequent expansion through the exit, or secondary nozzle) the MGD section, in some runs, was of constant cross-sectional area with parallel walls and an easily removable inlet and exit nozzle. When the exit nozzle was present, the observed thrust was always higher.

When only MGD effects were sought, the exit nozzle was omitted. When maximum conversion of energy into thrust was desired, the nozzle was included. The results presented in this paper are based on experiments in which the inlet and exit nozzle were omitted.

Electromagnet

The magnet gap can be varied from 0 to 3 in. by sliding the 3-in.-diameter pole pieces in or out on the yoke. The ends of

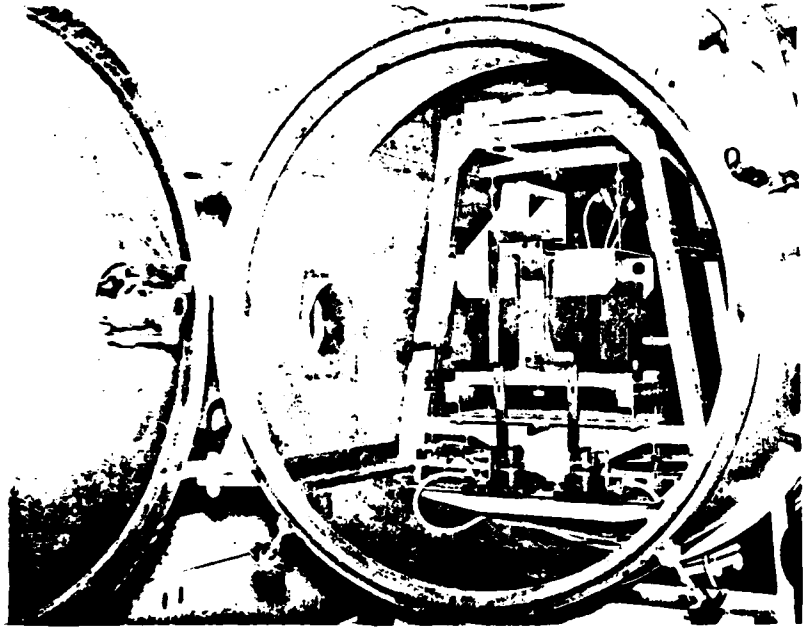

Fig. 3. View of MGD driver on balance in vacuum tank

Plasma generator mounted on tank door at left.

the pole pieces can be replaced by tips of various shapes, coated with zirconium oxide, to give magnetic fields of various geometries including a divergent gap. The pole pieces can be removed completely to facilitate observation of the discharge region between the electrodes. With the magnet pole pieces removed, a magnetic induction of up to 4000 gauss could be obtained in the MGD driver. The magnet current could be regu-

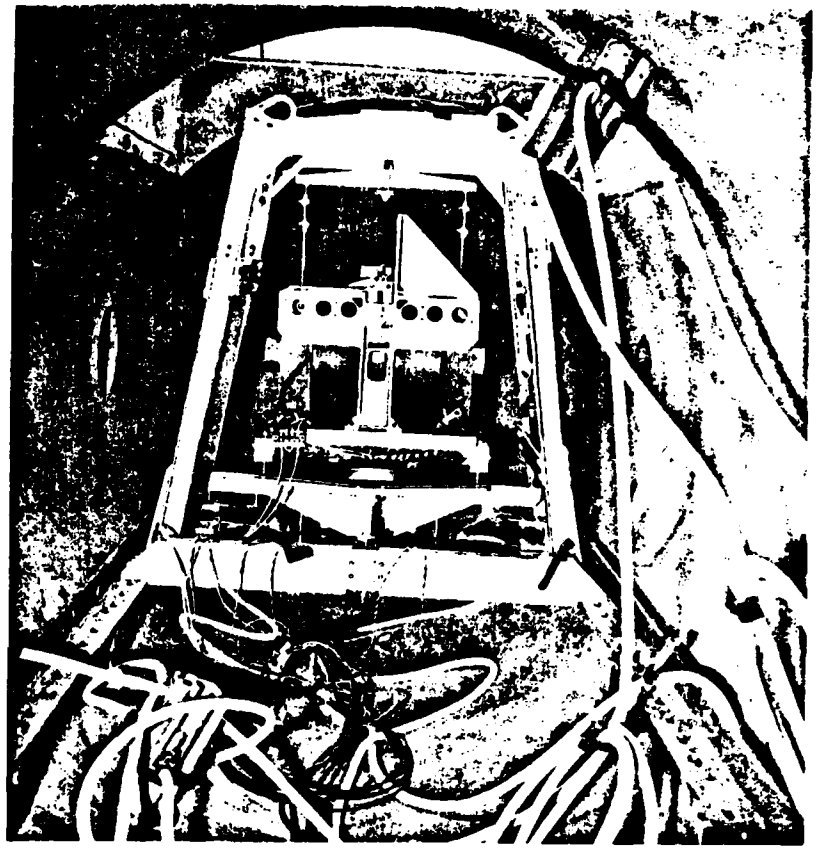

Fig. 4. Rear view of MGD driver in vacuum tank

lated from 0 to 7 amp dc with less than 2% ripple. Higher current levels were provided by batteries.

Electrodes

The electrode gap could be varied from 0 to 4 in. by sliding the electrodes in and out of their holders. Finer adjustments are possible by moving the holders themselves. Various electrode materials (molybdenum, pure or thoriated tungsten, etc.) and configurations were tested. Some of these configurations were the segmented electrode, the serrated electrode, the multipoint-separate power-supply electrode, and the rotating elec-

trode. Electrode cooling was accomplished by means of an integral aluminum heat sink which doubled as electrode holder. Figures 5, 6, and 7 show various electrode configurations tested in the course of this investigation.

Thrust Balance

In order to measure directly the thrust developed by the MGD driver, the entire magnet-electrode assembly is mounted on a balance system capable of reading thrust within 1/5 oz. This balance consists of a platform mounted on a spike under the c.g. (in later versions two spikes on a plane containing the c.g. and the magnet pole piece axis) which rests in a shallow depression on a carriage. The carriage can slide along on rails, firmly emplaced in the walls of the low-pressure tank containing the balance-MGD driver assembly, and can be clamped at a position which gives sufficient separation between the MGD driver and the plasma jet nozzle exit. The carriage position can also be adjusted to line up the plasma jet and MGD driver axes.

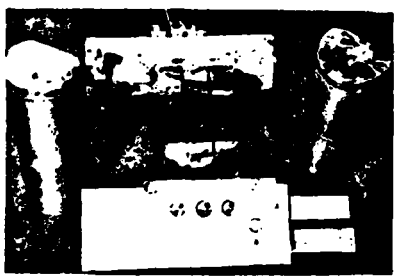

Fig. 5. Segmented electrode assembly and magnet pole pieces

The weight of this assembly on the spike is counterbalanced by use of an overhead ball fulcrum with three degrees of freedom tensioned by a bungee cord. The overhead fulcrum is supported by a frame which is an integral part of the sliding carriage. Thus, only part of the MGD driver weight rests on the pointed bottom spike or fulcrum. Any thrust or drag on the balance tends to make the balance tip around the bottom fulcrum before the motion begins to be constrained by the top fulcrum. Strain gauges, with one end fixed on arms extending from the platform and the other end fixed to the tank walls, measure the forces on the balance in three directions, forward and backward (thrust and drag), right and left (side forces), and up and down (lift forces). Since no significant side or lift forces were detected in preliminary experiments, later versions of the balance (resting on two spikes) measure only thrust or drag. The strain gauges are calibrated by applying known loads to the MGD section, through a pulley, to simulate thrust and drag. Balance damping was provided by means of an oil dash-pot.

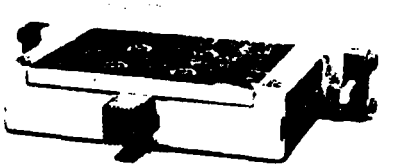

Fig. 6. Serrated electrode assembly

A deflection vane or ballistic pendulum was also used to measure the momentum of the exhaust. It should be noted, how-

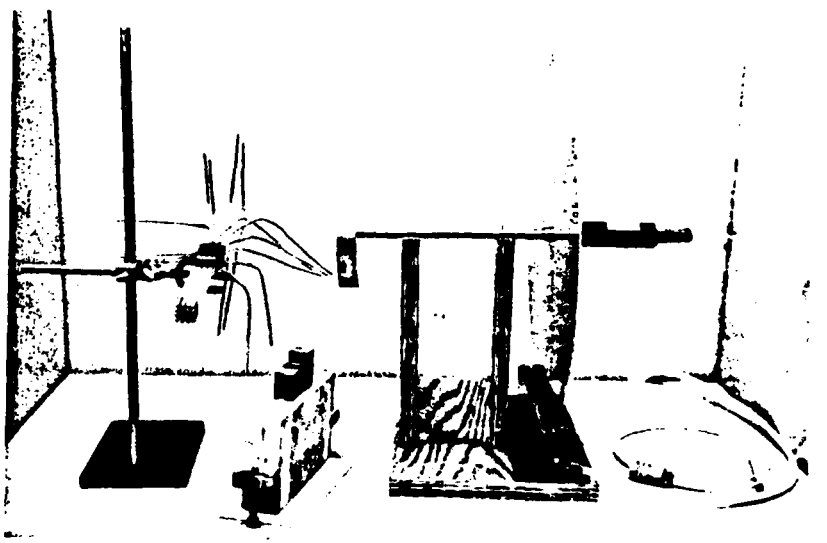

Fig. 7. Various electrode configurations

Pincushion or multipoint with separate power supplies (left), serrated step (center), rotating electrode (right).

ever, that the latter measurements are not as reliable and should be corrected for various effects.

Plasma Generator and Plasma Velocity Measurements

A commercial gas-stabilized electric arc jet with a supersonic head is used to generate the plasma. The velocity at the exit of this plasma generator is very nearly uniform. Plasma velocity at the MGD driver inlet is measured by discharging a small, but intense, spark in the plasma upstream of the MGD driver, and determining the time of travel to one or more downstream stations while the MGD driver is not operating. The spark discharge increases the local luminosity of the gap and this disturbance is monitored by shielded photomultiplier tubes at several stations along the plasma stream. Output signals are displayed on an oscilloscope and recorded with a polaroid camera. Velocities at the exit of the plasma generator are also supplied by the manufacturer's calibration charts.

EXPERIMENTAL RESULTS

When the electric current and magnetic induction were turned on while the plasma jet was streaming through the space confined by the pole pieces and the electrodes, a definite reaction, either thrust or drag, depending on polarity, was detected by the balance.

The following qualitative tests were used as criteria to establish the nature of this effect:

1. With the current on (apparently due to field emission of electrons) and the magnet off, there was no detectable balance reaction. When the magnet was switched on there was a definite reaction of thrust or drag, depending on the polarity of the magnetic field.
2. Reversing the polarity of the magnet caused the force on the balance to reverse direction.
3. As the magnetic field was increased, the current passing through the electrodes decreased, until at a certain value of the magnetic induction the discharge was extinguished.
4. As the magnetic field was increased the voltage between the electrodes increased due to the falling-voltage characteristic of the power supplies (batteries or motor-generators).
5. When the externally applied electric field was switched off, i.e., when there was no discharge or applied electric current between the electrodes, while the magnetic field was on, an emf was generated between the two electrodes and a current flowed in the circuit (heating a resistance).
6. When the plasma was turned off and the electrodes were made to touch or were otherwise shorted through a rigid path, so that an applied current flowed while the magnetic field was turned on, there was no detectable reaction of the balance.
7. The visible discharge between the electrodes of the MGD driver became thicker as the current density increased.
8. An increase in the electrode current at constant magnetic induction caused a proportional increase in the thrust.
9. No evidence exists to indicate that entrainment of ambient gases or other matter caused an increase of the thrust of the MGD driver.

Several other qualitative effects observed during the course of these early investigations are worth mentioning. It was found that the trailing edge of the anode was first to glow and that the glowing region spread upstream and down the anode stem in a cylindrical front with the trailing edge for an axis. This indicates that the discharge probably stabilizes at the anode trailing edge. It was found that the hot luminous core of the plasma jet could be a considerable distance (of the order of 1/4 in.) from the electrode surfaces without impairing the flow of current. This could imply that the luminous core of the jet is surrounded with a conducting sheath due to the diffusion of electrons. The momentum of the particles in the conducting sheath appears to be lower than the momentum of the particles in the core. A deflection of the jet, due to the Lorentz forces caused by Hall currents interacting with the magnetic field, was also observed.

Other qualitative results included the increase of the apparent conductivity of ionized streams (without raising the static temperature) by the application of glow or electrodeless discharges, and the increase of the apparent thermionic emission of various surfaces by irradiation with microwaves in the 2400 Mc region.

The quantitative results include the continuous measurement on synchronized recorders of the thrust or drag (two calibrated strain gauges of appropriate sensitivity), magnet-coil current (measured by means of a current shunt; calibration curves give the induction in the gap), electrode current (calibrated current

shunt), voltage across the electrodes, ambient tank pressure (Pirani gauge calibrated against a McLeod gauge), pressure and temperature at selected points in the MGD driver, arc jet current and voltage, and arc jet flow rate. The data are recorded continuously on strip charts by means of Sanborn 850 recorders. This approach has two advantages: it allows more direct attention to operation of the actual experiment and permits a permanent record to be kept for later data analysis without any question of event synchronization. Usually the electrode power supply output is set before the experiment. The electrode current is turned on first; then the magnet is switched on and the magnet current is adjusted manually to give the desired thrust level.

Present Range of Experiments

The electrode current was varied from 10 to 2000 amp/in.^{2}. The electrode potential difference was varied from 24 to 360. The geometric-average electric fields varied from 24 to 360 v/in. The plasma generator power was varied from 30 to 150 kw. The electrode gap was varied from 0.80 to 2.25 in. The magnet gap was varied from 1 to 3 in. The magnetic induction was varied from 0 to 5000 gauss. Typical measurements (Fig. 8) were: argon flow rate, 1.40 g/sec; electrode gap, 1.40 in.; electrode current, 470 amp; electrode voltage, 51 v; magnetic induction, 700 gauss; net MGD thrust increment, 0.25 lbf (identical on both gauges); and plasma velocity at inlet of MGD section, approximately 12,000 ft/sec (from plasma generator calibration). On the basis of these measurements the computed ideal thrust increment is 0.26 lbf and the MGD driver efficiency is 28%. The agreement between measured and computed thrust is excellent.

In less typical runs (Fig. 9), where the electrode gap was smaller so that visible oblique shocks were formed at the leading edge of the electrodes, the measurements yielded: argon flow rate, 1.37 g/sec; electrode gap, 1.19 in.; electrode current, 580 amp; electrode voltage, 80 v; magnet gap, 2.68 in.; magnet current, 5 amp (calibration charts give an induction of 0.3 weber/m^2); net MGD thrust increment, 0.562 lbf (identical on both gauges); and argon plasma velocity, approximately 12,000 ft/sec. On the basis of these measurements the computed ideal thrust increment is 1.18 lbf. Therefore, the measured thrust is only 48% of the ideal thrust and the driver propulsion efficiency is approximately 24%.

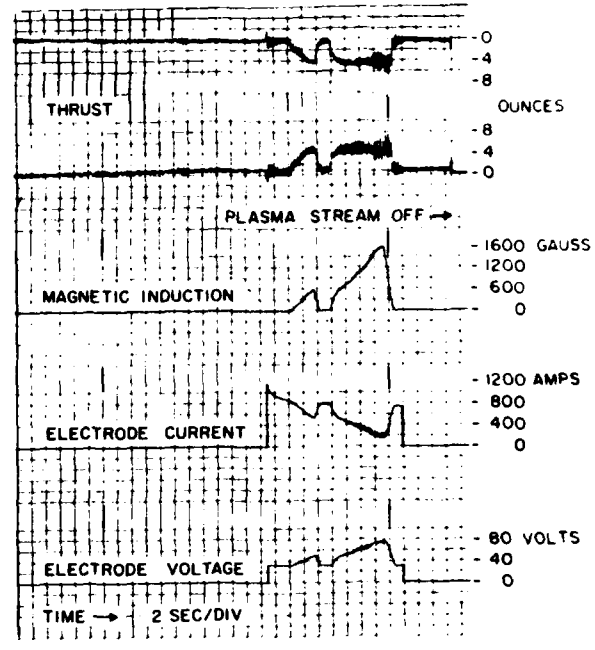

Fig. 8. Typical early test of Northrop MGD driver

Argon expellant at 1.40 g/sec; electrode gap, 1.40 in.; battery power supplies; efficiency, ~28%.

Duration of runs is currently up to 60 sec but can be increased to 5 min. Thrust increments of up to 3 lbf with argon and up to 1.25 lbf with nitrogen were obtained before reaching the continuous-rating limitations of present power supplies. It appears possible to increase the thrust of the present MGD engine even further by use of power supplies with higher current and voltage output.

Experimental Results with Argon

Typical records of early tests of this MGD engine with argon expellant are shown in Figs. 8 and 9. Note that the drag of the plasma jet on the electrodes and the gasdynamic (thermal) thrust due to heating of the plasma by the electrode current (the electrodes were not mounted flush with the channel walls) are clearly shown in Fig. 9. The initial drag, due to impingement of the jet on the electrodes and the resulting oblique shocks, is approximately 1 oz and it appears as soon as the plasma stream is turned on. The drag takes approximately 7 sec to build up to

a nearly constant value as the power is brought up to the desired level. Approximately 20 sec after the plasma jet is turned on, the electrodes are switched on and an initial current of 1200 amp surges through the motor generator. The energy added to the plasma increases the temperature and pressure of the supersonic stream and the increased pressure forces acting on the rear wall of the protruding electrodes cause a thrust which, after the transients have died out, just about cancels the electrode drag. Thus, the *net* gasdynamic or thermal thrust is nearly 1 oz and can be clearly identified. Three seconds after the current is turned on it reaches a nearly constant value and 2½ sec later the magnetic field is switched on. As the magnetic field is increased (by increasing the magnet current manually)

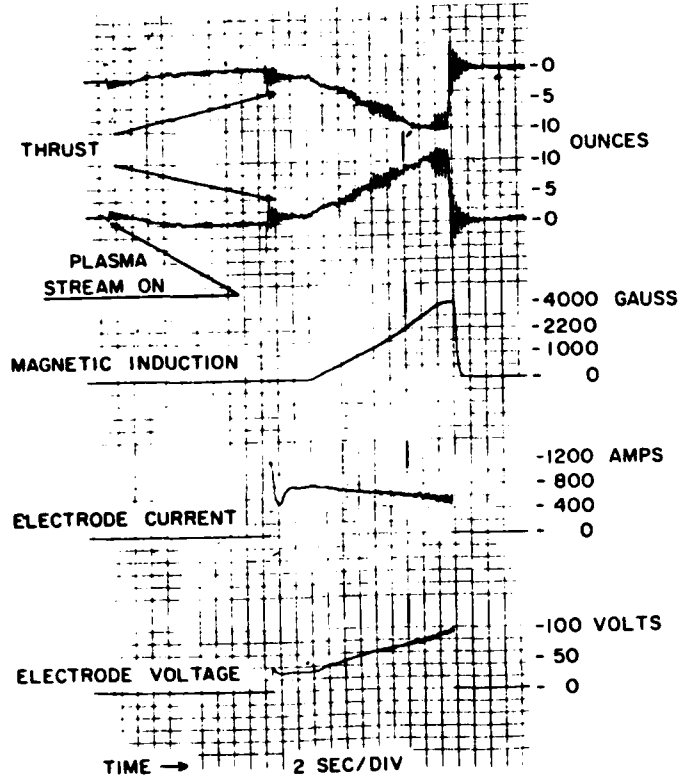

Fig. 9. Typical early test of Northrop MGD driver

Argon expellant at 1.40 g/sec; electrode gap, 1.19 in.; motor generator power supply; efficiency, ~25%.

the MGD or Lorentz thrust begins to increase while the electrode current goes down and the electrode voltage goes up. However the MGD thrust does not increase quite as fast as it should because part of the current passes through the plasma thrown outside the region of magnetic influence by the oblique shock. Finally, the thrust reaches a value of approximately 10 oz at 3800 gauss; then it begins to decrease with an increase of the magnetic field. Note that the flattening out of the induction curve near the peak of 4000 gauss is due to the limit on the travel of the recorder pen. The actual induction in the last 2 sec increases well above 4000 gauss. The electrode current is then switched off and, almost simultaneously, the magnet current is turned down to zero.

Figure 8 was a similar record of events during a run which used batteries to supply the power. Note the steeper decrease of the current with an increase in induction, and the effect of internal heating on the battery output. In this run the magnetic induction was increased and brought back to zero twice. The magnet current was finally turned off before the electrodes were switched off. The electrode current, however, did not come back to its exact original value because of the effect of the overload on the batteries.

Figure 10 gives the measured performance characteristics of an early MGD driver for argon. Figure 11 gives the measured thrust of an MGD engine for argon as a function of magnetic induction for various electrode currents. Note that the difference between the measured thrust and the ideal thrust increases with an increase in magnetic induction. This is probably due to an increase in the Hall currents.

In all the argon runs plasma generator power varied from 30 to 100 kw and the plasma velocity at the inlet of the MGD driver was within the range 10,000 to 14,000 ft/sec. The value of 12,000 ft/sec was used to compute the efficiencies of Fig. 10. Using 10,000 ft/sec reduces the propulsion efficiency from 38% to 33%. The plasma generator cooling rate was not measured in each run and so it is not possible to estimate the plasma jet velocity with greater precision. However, the plasma jet is usually underexpanded, i.e., there is additional expansion between the exit nozzle and the plasma jet inlet and therefore the higher values may be justified.

The oscillations which appear on the thrust records are due mostly to the reciprocating pump used to maintain the tank pres-

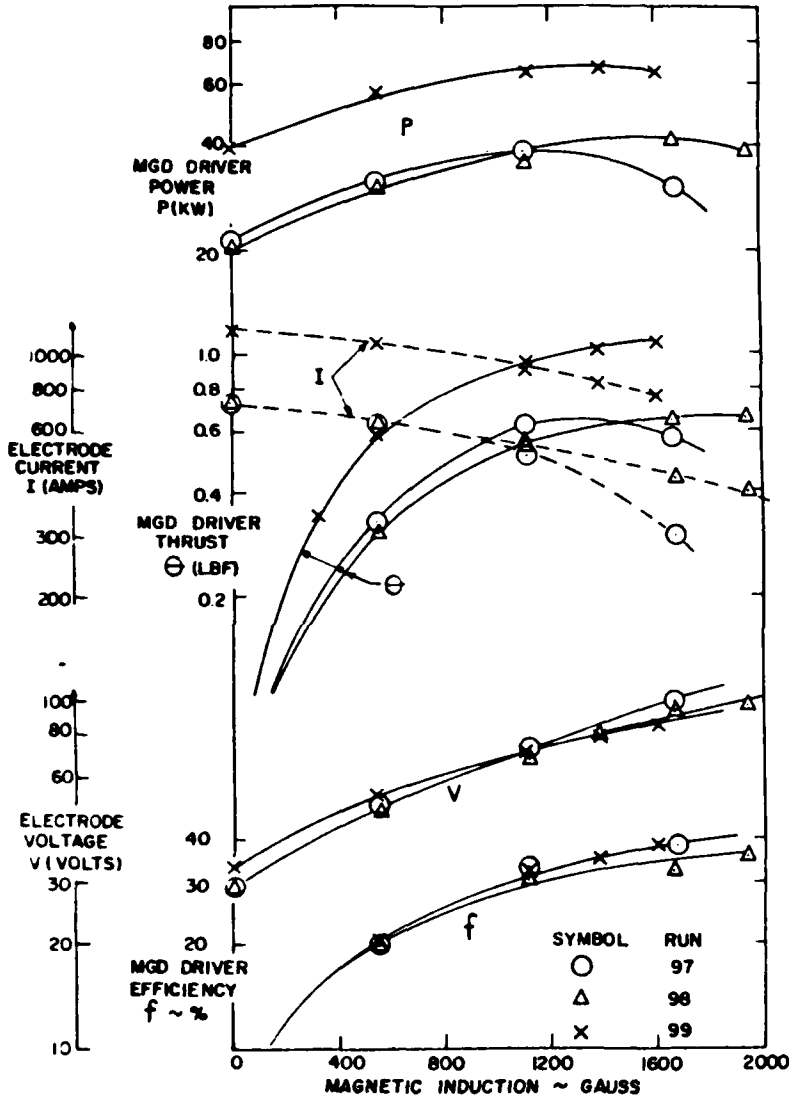

Fig. 10. Performance characteristics of early MGD driver for argon

No exit nozzle; electrode gap, 2 in.; motor generator power supplies; argon flow rate, 1.4 g/sec.

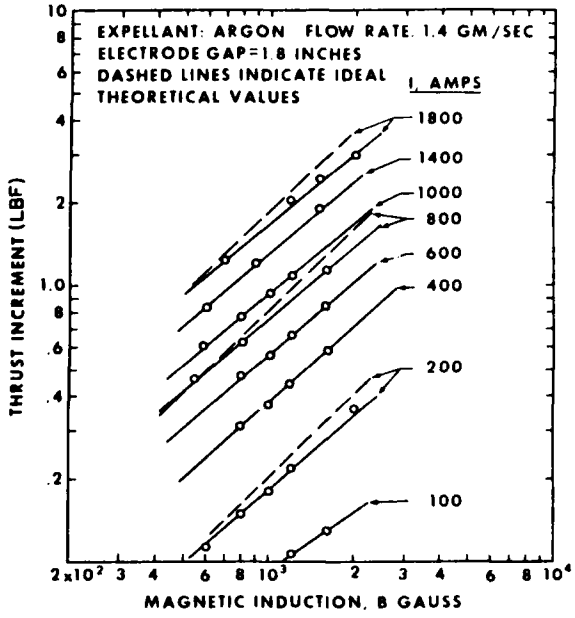

Fig. 11. Thrust increment of MGD driver as a function of magnetic induction for different electrode currents

sure of 2000 μ. However, in some cases an increase of the magnetic induction caused an instability of the electrode discharge (which manifested itself in a broadening of the current and voltage traces). This discharge instability preceded the critical induction value at which the discharge was extinguished and made it possible to operate in a stable current-induction regime.

It is quite possible to improve the specific impulse and efficiency (current values 1400 lbf-sec/lbm and 40%, respectively) of the MGD engine for argon by operating at higher currents and inductions. An efficiency of this engine of 80% or better does not appear impossible with further development.

Experimental Results with Nitrogen and Air

The recordings of thrust and other performance characteristics of this MGD engine, using air and nitrogen as expellants, exhibit a behavior similar to the argon recordings (Figs. 8 and 9). The only notable difference is that in the nitrogen runs the current instability can be induced at a lower magnetic induction

and the critical induction is smaller than for argon. This is due to the lower conductivity of the nitrogen and air plasmas, the high recombination rates for nitrogen compared to argon, and also to the higher velocity of these plasmas at the inlet and throughout the MGD section. The velocity of the nitrogen and air plasmas at the inlet of the MGD driver ranges from approximately 12,000 to 18,000 ft/sec. Therefore, the field due to the induced back emf, given by the integral

$$B_o \int_0^L U_x dx,$$

can be 40% higher than for argon. These difficulties can be overcome by operating the plasma generator at higher power levels (or irradiating the nitrogen or air plasmas with microwaves) to increase the conductivity, by decreasing the distance between the plasma generator and the MGD driver, and by operating the electrodes at a higher electric potential. Operation at higher potential, however, will decrease the efficiency unless accompanied by an increase of conductivity.

Figure 12 gives the measured performance characteristics of an early MGD driver for nitrogen and air. Figure 13 gives the measured thrust of an MGD engine for nitrogen and air as a function of the magnetic induction for various electrode currents. Note that the efficiency of this engine is lower than the efficiency of the same engine using argon.

The value of the nitrogen or air plasma velocity at the inlet of the MGD driver used in the computation of the propulsion efficiency was 17,000 ft/sec. Using 12,000 ft/sec reduces the efficiency from 17% to 12%. The plasma jet power settings in the nitrogen runs varied from 80 to 150 kw.

Considerable and destructive oxidation of the fixed electrodes was encountered, as expected, during the runs when air was used as expellant and, therefore, the air runs were limited to less than 20 sec. The oxidation problem can be solved by operating the electrodes at low temperatures (cooling or spinning) and using oxidation-resistant metals.

DISCUSSION OF RESULTS

At least in the low-current low-induction region the thrust measurements are in good agreement with the idealized theory of Eqs. (1) and (2), i.e., the measured thrust is within 10% of

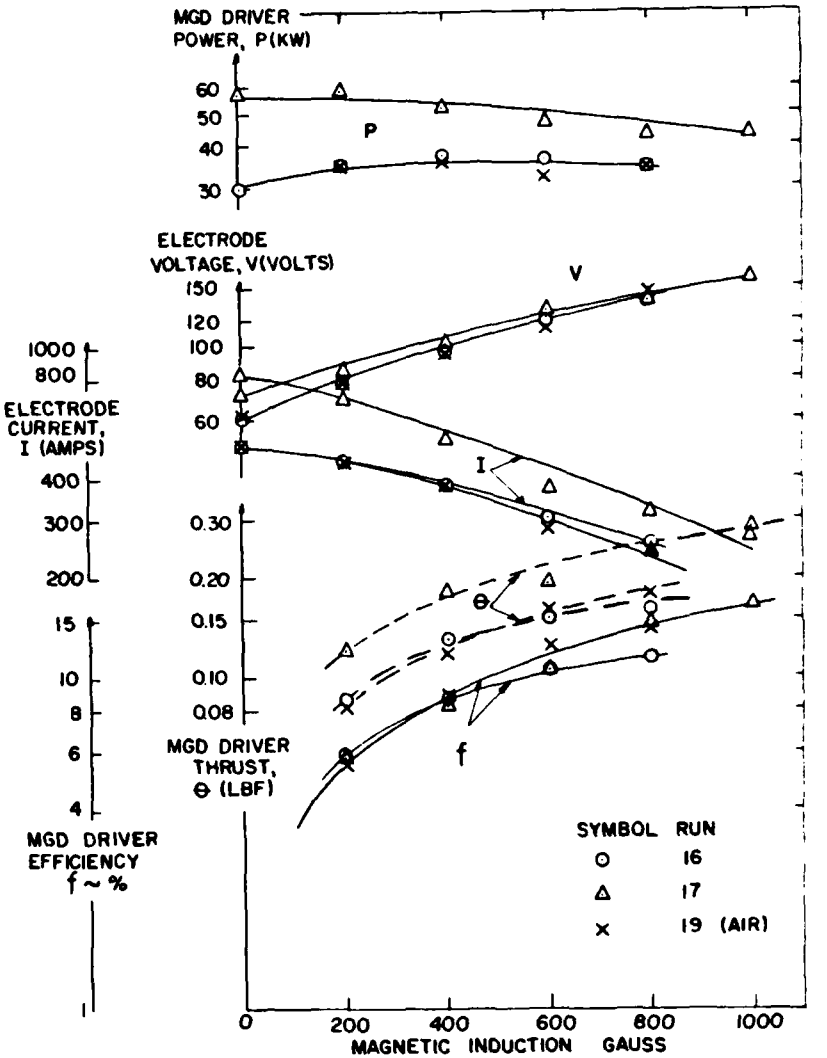

Fig. 12. Performance characteristics of early MGD driver for nitrogen and air

No exit nozzle; electrode gap, 1.80 in.; motor generator power supplies; flow rate, 1 g/sec.

the computed value. Thrust values are presented in terms of total current rather than conductivity in order to avoid the difficulties associated with measuring conductivity. The electrodes

are operated at high current densities of the order of 1000 amp/in.^{2}. Electron field emission appears to be the principal mode of operation. The combined effects of plasma velocity and space charge must be such that the electric field is smaller near the anode, and much greater near the cathode, than the

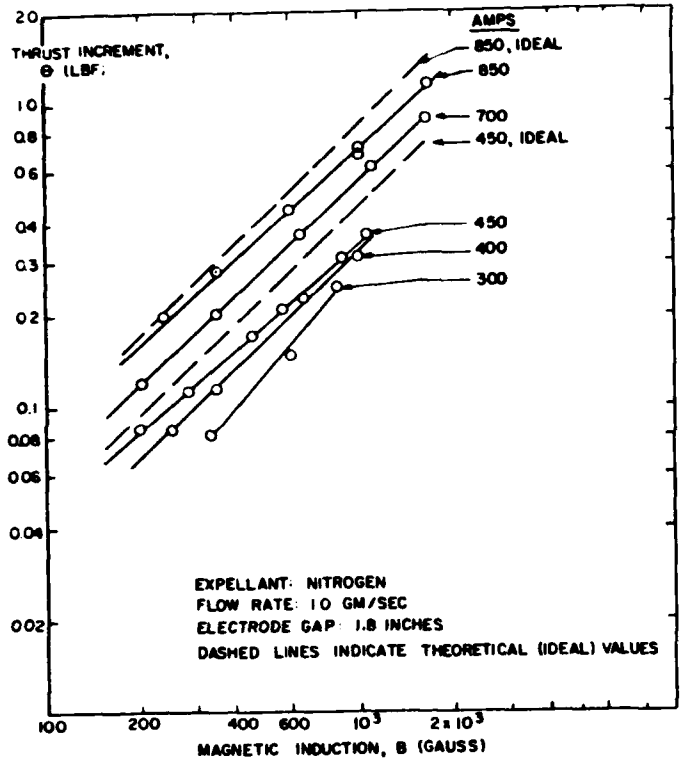

Fig. 13. Thrust increment of early MGD driver for nitrogen as a function of magnetic induction for different electrode currents

geometrical (uniform distribution) field. The high electric microfield then gives rise to a Schöttky effect which accounts for the high current densities that have been observed at these low geometrical fields. Electrodes which combine long endurance with stable operation and high current densities are required for efficient continuous-flow MGD engines; electron field emission rather than thermionic emission appears to offer most promise.

A set of serrated tungsten electrodes (Fig. 6) has been operated intermittently with argon and nitrogen at current densities in excess of 300 amp/in.^{2} for a total of several hours without any apparent erosion. Other electrodes, notably segmented (Fig. 5) and multipoint (Fig. 7) electrodes with separate power supplies for each segment or point, have also been operated. The results to this date have not brought out any conclusive advantages for any one of these three types of electrodes. The rotating or spinning electrode shown in Fig. 7 is more or less a laboratory curiosity at this stage. It was devised to test the theory[15] that intermittent exposure of the electrode surface to the hot-air plasmas would reduce erosion and surface oxidation by lowering the surface temperature of the electrode at the point of contact with the jet (at a rate higher than is possible by mere heat transfer) and by reducing the time of exposure of a given part of the surface to the plasma. Preliminary results indicate that erosion and oxidation can be suppressed by use of this electrode with air. Further work is required to increase the ionization by means of "cold" (electrodeless or glow) discharges. There the problem appears to be one of coupling the discharge to the plasma. Further work is also required to remove all uncertainty from the MGD driver inlet velocity measurements.

The concentration in the plasma jet is approximately 10^{16} particles/cc. Assuming that the plasmas in these engines are 1% ionized, the simple relationships given by Janes and Fay[16] for the product $\omega\tau$ (where ω = electron cyclotron angular frequency, τ = mean electron collision time) and the "ion slip" condition can be applied. Then

$$\omega\tau \approx 10^{-1} B (P_o T/PT_o) \tag{6}$$

and

$$B_p \leq 10^2 (PT_o/P_oT), \tag{7}$$

where B_p is the permissible field for negligible ion slip in weber/m^2, P_o = 1 atm, T_o = 0°C, P = static pressure in the plasma, and T = static temperature in the plasma. For $P = 2 \times 10^{-3}$ atm and T = 3000°K, $\omega\tau = 5 \times 10^2 B$, weber/m^2 and $B_p \leq 2 \times 10^{-2}$ weber/m^2. The results obtained by Janes and Fay imply[16] that an increase of the magnetic field of this engine above 200 gauss would not be useful since the ions then would "slip" between the neutral particles without effectively accelerating them by collisions. Berner and Camac[17] state: "There

is thus an upper limit to the forces that may be exerted on the gas as a whole and there is nothing to be gained by going to magnetic field strengths which exceed this limit." All these authors[16],[17] imply that, because of ion slip, the magnetic field of the MGD engine reaches a value beyond which any additional increase in B does not bring about any increase in thrust but only a decrease of MGD engine propulsion efficiency.

This is not necessarily true, since, as long as the electrons interact with the magnetic field they are accelerated (and the ions with them) and thrust is obtained irrespective of ion slip. In other words, ion slip is not a real limitation on MGD driver thrust, although under certain conditions it may be a limitation on neutral-particle velocity. In any case, no leveling off of thrust has been observed until inductions at least an order of magnitude greater than 200 gauss were attained; then leveling off or decrease of thrust was due to the decrease in total current. No decrease of the engine propulsion efficiency with increasing B has been observed in the range of magnetic inductions studied thus far. In fact, all indications are that an increase in efficiency should be expected at higher magnetic fields, with continued development, since the thrust power at constant current increases with the square of the magnetic field.

Other sources of inefficiency, such as boundary layer losses, appear to be smaller than is indicated by current diligent, but unrealistic, theoretical work. In fact the low-momentum conducting sheath that appears to surround the plasma jet may lead to devices which are not viscously contained in the ordinary sense of the word. Typical measurements of momentum and effective conductance in the low-momentum sheath appear in Fig. 14. There appears to be no reason why the plasma jet should be in actual contact with the magnet pole faces for efficient engine operation, and the electrodes need only be immersed in the low-momentum conducting sheath. Many runs have been made with the free-jet arrangement. However, even when the plasma impinges on all four surfaces (two pole pieces and two electrodes) of the MGD driver, the viscous drag appears to be less than is indicated by current boundary-layer theories. In addition to the findings concerning the low-momentum high-conductivity plasma sheath, the experimental results obtained with this device indicate that a stable discharge can be achieved with electron field emission, that ion slip imposes

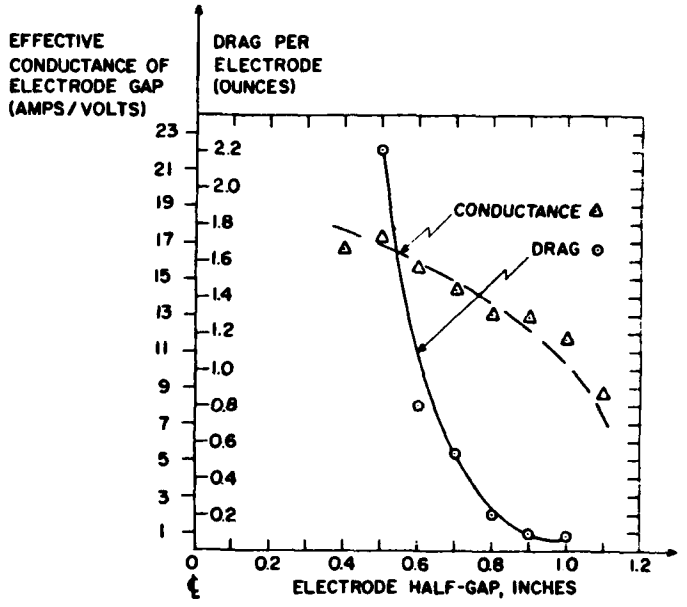

Fig. 14. Typical measurements of momentum and effective conductance in the low-momentum sheath

no serious limitation on thrust and the Larmor radius imposes no serious limitation on total current below 4000 gauss, and that the electron temperature and degree of ionization in the engine are an order of magnitude higher than that imposed by thermal equilibrium.

FURTHER THEORETICAL RESULTS

As empirical knowledge begins to accumulate on MGD propulsion engines, theoretical analyses will become more and more realistic. Recent work in this laboratory has treated the problem of variable-area magnetogasdynamic channel flow.[18],[19] Solutions have been presented for the case of constant instantaneous conversion efficiency and for the case of constant temperature. These solutions are not restricted to constant applied electric fields and are consistent with the Maxwell equations. The fluid and field variables are obtained in terms of the axial coordinate and/or the fluid velocity. On the basis of these results, operating characteristic plot (OCP) and performance envelopes are derived for argon, nitrogen, and air at various de-

grees of equilibrium and nonequilibrium ionization. These curves consist, for example, of a plot of ideal power versus exhaust density (or magnetic induction, or channel length or current density or power density) for various aspect ratios or heights of the MGD channel, various magnetic Reynolds numbers, various degrees of departure from thermal equilibrium ionization, various degrees of magnetic field loss, boundary layer loss and electrode loss, various magnetic inductions, various Alfvén Mach numbers, etc.

It was concluded that departure from thermal equilibrium ionization extends the desirable range of operation of MGD drivers (accelerators or engines) into regions which, hitherto, were considered prohibited, and alleviates thermal loss problems. "Cold" plasma operation of the MGD driver appears feasible and desirable. Electron temperatures an order of magnitude, or more, higher than the stream static temperature are to be expected, and the degree of ionization should be much higher than that indicated by equilibrium computations at stream temperature. The implications of the theoretical and experimental results are that magnetogasdynamic engines of high efficiency and long and stable engine life are possible. The same can be said of MHD power generators when the kinetic energy or enthalpy of the fluid is divorced from the ionizing energy, i.e., when the main thermal energy source is used to drive the fluid and an other-than-thermal energy source is used to produce the high degree of ionization.

Further experiments are planned to test the validity of this work.

CONCLUSIONS

Direct and unambiguous measurements of MGD thrust were obtained with a continuous-flow MGD engine mounted on a balance. The engine was of rectangular geometry and used steady crossed fields. Argon, nitrogen, and air were used as expellants and the electrodes were successfully operated in the field emission regime. The thrust of an argon plasma jet was augmented by 200%.

Although an uncertainty of 15% exists in the propulsion efficiency measurements with argon expellant, nevertheless, the MGD efficiency obtained, excluding the plasma generator, is greater than 30% for argon. An uncertainty of 40% exists in the

propulsion efficiency measurements with nitrogen or air expellants. However, the MGD engine efficiency obtained with nitrogen or air is greater than 10%. No specific attempt was made to optimize the geometry or efficiency of this MGD engine.

The uncertainty in the efficiency measurements can be removed either by mounting the plasma generator on the balance along with the MGD driver or by direct and continuous measurement of the plasma generator exhaust velocity or cooling losses. Both these approaches are now being pursued at the Space Propulsion and Power Laboratory of the Northrop Corporation.

ACKNOWLEDGMENTS

I want to thank the Northrop Corporation for making funds available for this study. I also want to thank Mr. Norman V. Petersen for his moral support and encouragement, Professors J. R. Pellam and R. P. Feynman of the California Institute of Technology and Raymond Chuan of the University of Southern California for helpful discussions, Dr. R. W. Ziemer who helped solve some of the instrumentation problems in recent months, Mr. C. F. Young for checking the reduction of data, and the laboratory technicians J. Superata, L. Goltra, and C. Hohn who helped me assemble and operate the apparatus and obtain the first thrust measurements on May 27, 1960.

REFERENCES

1. S. T. Demetriades, "Magnetogasdynamics and space propulsion," ASL-TM-60-33, Norair Division, Northrop Corporation, Hawthorne, California; presented at the First Symposium on Engineering Aspects of Magnetohydrodynamics, February 18–19, 1960; published in part in Western Aviat. Mag. *40*, 14 (1960).
2. S. T. Demetriades, "A Novel system for space flight using a propulsive fluid accumulator," NB-59-161, Norair Division, Northrop Corporation; ASTIA Doc. AD-226-086, December 20, 1958; J. Brit. Interplanet. Soc. *17*, 114 (1959).
3. S. T. Demetriades, "Magnetogasdynamic acceleration of flowing gases and applications," NB-59-153, Norair Divsion, Northrop Corporation; ASTIA Doc. AD-226-672, March 23, 1959; Nuclear Science Abstracts, USAEC Tech. Info. Service, Vol. 14, No. 10, abstract No. 10114, May 31, 1960.
4. S. T. Demetriades, "New propulsion concepts," NB-159-176, Norair Division, Northrop Corporation; ASTIA Doc. AD-226-057, July 1, 1959.
5. S. T. Demetriades, "Orbital propulsion system for space maneuvering (PROFAC)," Aero. Sci. Rev. *1*, 17 (1959).

6. S. T. Demetriades, "Design and applications of propulsive fluid accumulator systems," NB-60-16, Norair Division, Northrop Corporation, February, 1960; also AFBMD-TR-60-14, Part III, February, 1960.
7. S. T. Demetriades, "Preliminary study of propulsive fluid accumulator systems," ASRL-TM-60-7, Norair Division, Northrop Corporation, June, 1960; also presented at XIth IAF Congress, Stockholm, Sweden, August 15–20, 1960, paper No. 53.
8. W. J. Franke, "Design of a dissipative inlet for PROFAC," RASR-60-23, Norair Division, Northrop Corporation, September, 1960.
9. S. T. Demetriades, "Magnetohydrodynamic orbit control for satellites," ASRL-TM-60-6, June, 1960; also presented at AIEE General Meeting, August 8–12, 1960 (CP 60-1087); Elec. Eng. *79*, 987 (1960).
10. S. T. Demetriades and C. F. Young, "Orbital refuelling satelloid," paper No. 230H, SAE AFOSR Astronautic Symposium, Los Angeles, October 12–14, 1960.
11. S. T. Demetriades and C. B. Kretschmer, "Preliminary investigation of an atomic-oxygen power plant," Aerojet- General Corporation, TN-23, AFOSR TN-58-325, ASTIA Doc. AD-154-229, March 4, 1958; summarized in J. Aero/Space Sci. *25*, 653 (1958); also in Am. Rocket Soc. J. *29*, 375 (1959).
12. S. T. Demetriades and C. B. Kretschmer, "The use of planetary atmospheres for propulsion," presented at the Fourth Annual Meeting of the AAS, New York, January 31, 1958; paper No. 46; AFOSR TN-58-229, ASTIA Doc. AD-154-132, April 14, 1958.
13. A. F. Charwat, "Photochemistry of the upper atmosphere as a source of propulsive power," Am. Rocket Soc. J. *29*, 108 (1959).
14. S. T. Demetriades, "Energy transfer to a nitrogen plasma," NB-60-311, November, 1960; "Electrodes for MGD engines," NB-60-319, January, 1961, Norair Division, Northrop Corporation.
15. S. T. Demetriades, "Theory of heat transfer from hot steady or intermittent supersonic jets," NB-59-152, Norair Division, Northrop Corporation; ASTIA Doc. AD-226-085, March 16, 1959.
16. G. S. Janes and J. A. Fay, "Magnetohydrodynamics acceleration of slightly ionized, viscously contained gases," presented at the Second Symposium on Advanced Propulsion, Boston, October 7–8, 1959.
17. F. Berner and M. Carmac, "Air scooping vehicle," Avco-Everett Research Laboratory, Research Report 76, AFBMD TR-59-17, August, 1959.
18. R. R. Berlot, "Some explicit solutions for constant-temperature magnetogasdynamic channel flow," ASL-TM-60-30, Norair Division, Northrop Corporation, October, 1960.
19. S. T. Demetriades and C. F. Young, "Operating characteristics of continuous MGD engines," ASG-TM-61-6, to be published.

END

FILMED

10-85

DTIC